CHAPTER 3

Mineralization of Phenol in an Improved Photocatalytic Process Assisted with Ferric Ions: Reaction Network and Kinetic Modeling

Aaron Ortiz-Gomez[1,*], **Benito Serrano-Rosales**[2], **Jesus Moreira-del-Rio**[1], and **Hugo de-Lasa**[1]

Contents

[1] The University of Western Ontario, London, Ontario, Canada

[2] Universidad Autonoma de Zacatecas, Zacatecas, Mexico

[*] Corresponding author.
E-mail address: aortizg2@uwo.ca

Advances in Chemical Engineering, Volume 36
ISSN 0065-2377, DOI: 10.1016/S0065-2377(09)00403-7

1. INTRODUCTION

1.1. Photocatalysis: a promising low-cost alternative

Every day, manufacturing industries produce water and gas effluent streams with significant amounts of organic and inorganic pollutants. Organic compounds in wastestreams include textile dyes, herbicides and pesticides, alkanes, haloalkanes, aliphatic alcohols, carboxylic acids, aromatics, surfactants, among many others (Guillard, 2003; Malato et al., 2004; Mukherjee and Ray, 1999). Inorganic compounds include complexes of metal ions such as mercury, cadmium, silver, nickel, lead, and other equally harmful species (Chen and Ray, 2001; Huang et al., 1996). Many of them are well known for their toxic effects on the environment and on human health. The elimination of these pollutants requires processes able to completely mineralize the organic pollutants and to convert the metallic contaminants into less harmful forms.

Heterogeneous photocatalysis has been proven to be a potential process to eliminate many of these hazardous organic pollutants present in air and water wastestreams and has therefore been the subject of extensive research over the last decades (Bahnemann, 2004; de Lasa et al., 2005). Photocatalytic (PC) processes, albeit advantageous for completely mineralizing complex harmful contaminants at relatively low cost (i.e., TiO_2 is inexpensive, 100–200 dollars per tonne; consumables are minimum, low lamp wattage or solar energy), take place at a rather slow rate. This has prompted the search of new means to improve their performance to tackle more efficiently the largely spread problem of polluted wastestreams. Owing to the particular characteristic of photocatalysis to produce nonselective hydroxyl radicals $HO^{\bullet}$, chemical species with high oxidative power, it was applied to environmental engineering for pollutant decontamination. Photocatalysis then emerged as a new process that could provide a solution to complete mineralization of organic contaminants and reduction of harmful inorganic metal ions.

Contaminants such as phenol, whose toxic effects on human health are well documented, have been widely used as a model pollutant to elucidate the complex PC reaction mechanisms and to evaluate the performance of

many reactors designs and catalyst activities (Tryba et al., 2006a, b) Moreover, phenol and similar hydroxylated compounds are well-known contaminants present in wastewater effluents from many industrial processes (US Environmental Protection Agency, 2000 and references therein). Their toxic effects on human health are well documented, being related to severe illnesses such as leukemia (McDonald et al., 2001) and some serious human organ malfunctions (ATSDR, 1998). They are highly toxic and refractory pollutants not easily removed in biological wastewater treatment plants (Goi and Trapido, 2001). Hence, PC processes need to be improved to provide highly efficient solutions for heavily contaminated wastestreams and to minimize human exposure to species such as those mentioned above.

1.2. Moving toward an improved process: minimizing inefficiencies

An important research approach to improve the PC process performance is the use of metallic complexes as additives in PC reactions. Some metallic compounds, such as Hg(II) (Aguado et al., 1995), Cr(IV) (Chenthamarakshan and Rajeshwar, 2000), Zn(II) (Chenthamarakshan and Rajeshwar, 2002), Cd(II) (Chenthamarakshan and Rajeshwar, 2002), among others (Huang et al., 1996; Tan et al., 2003), have been shown to modify the oxidation rate of organic species depending on their oxidation states and concentrations. Most of those metallic compounds tested so far are equally harmful or even more so than the targeted organic pollutants, preventing them from being used as reaction enhancers.

Another important approach is the structural modification and doping of photocatalysts with metals or dyes to increase their PC activity (Araña et al., 2004; Bamwenda et al., 1995; Colmenares et al., 2006; Dai and Rabani, 2002; Hufschmidt et al., 2002; Karvinen and Lamminmaki, 2003; Kim et al., 2005; Leyva et al., 1998; Nagaveni et al., 2004; Zhou et al., 2006). These doping techniques reportedly improve catalyst activity in some cases, leading to higher mineralization rates than the untreated photocatalysts. The preparation techniques, however, often involve complex procedures that call for expensive reactants as metallic sources and high temperatures for calcination steps, therefore hindering their usage and production for large-scale applications. Additional equipment must also be added to the process for catalyst recovery if the catalyst cost is a factor or to produce catalyst-free water if it is intended for human consumption. These additional costs could eliminate one of the greatest advantages of PC processes: the low catalyst cost and low operating costs. Thus, the search for means to improve the rate of mineralization of hazardous pollutants has veered off to look for inexpensive techniques that can enhance the PC processes using metallic complexes and yet be environmental friendly.

Extensive research has shown that of all PC materials, TiO_2 is the most active for oxidation reactions. Its higher catalytic activity, along with its low chemical and biological activity, low cost, and high stability has made it the best option for PC reactions (Fox, 1990; Fujishima et al., 2000; Ray, 1997). UV light with wavelengths lower that 388 nm can be absorbed by TiO_2 generating a pair of charges e^-_{cb}/h^+_{vb}. These charges can either recombine dissipating the absorbed energy or promote different reduction–oxidation (redox) reactions (Herrmann, 1999). The redox reactions to take place depend on the chemical species present in the vicinity of the catalyst surface or in the bulk of the solution (Fujishima et al., 2000; Turch and Ollis, 1990). The recombination of charges is one of the main drawbacks of PC processes as it leads to UV radiation usage inefficiencies. Thus, reducing the e^-_{cb}/h^+_{vb} recombination rates will result in higher production of hydroxyl radicals $HO^{\bullet}$ and consequently to higher oxidation rates.

1.3. Organic oxidation and inorganic reduction

Since photocatalysis was discovered in the early 1970s, more than 6,200 papers related to this process have been published. Most of the work on this subject has focused on showing that organic molecules can be oxidized in PC reactors. So far, more than 800 organic molecules have been tested for oxidation in PC reactions (Blake, 2001). In most cases, the tested organic molecules were converted to CO_2, water, and mineral acids. Therefore, it can be definitely concluded that photocatalysis works for oxidation of organic molecules. The rate of oxidation depends on several factors that will be addressed in the upcoming section.

More recently, during the last decade, it was found that some metal cations in water could be reduced using photocatalysis. It was proposed that the photogenerated electron could be used for reducing inorganic metal ions. For instance, Hg(II) was reduced to Hg(0) over TiO_2 suspensions (Aguado et al., 1995), as well as Cr(IV) to Cr(III) (Chenthamarakshan and Rajeshwar, 2000; Colon et al., 2001), Zn(II) to Zn(0), and Cd(II) to Cd(0) (Chenthamarakshan and Rajeshwar, 2002). Additionally, Ag(I) was also reduced to Ag(0) (Huang et al., 1996) and Se(IV) and Se(VI) to elemental Se(0) (Tan et al., 2003). Therefore, it was concluded that photocatalysis could be applied for metal cations reduction.

For a metal cation in water to be reduced with a photogenerated electron e^-_{cb}, its reduction potential must be less negative than the reduction potential of the conduction band. In this category fall pairs such as Ni(II)/Ni(0), Pb(II)/Pb(0), Fe(III)/Fe(0), Cu(II)/Cu(I), Cu(II)/Cu(0), Cu(I)/Cu(0), Fe(III)/Fe(II), Ag(I)/Ag(0), and Hg(II)/Hg(0). Figure 1 reports the reduction potential of different metals compared with both the valence band potential and the conduction band potential. All metals located above the conduction band can theoretically be reduced (Chen and Ray, 2001).

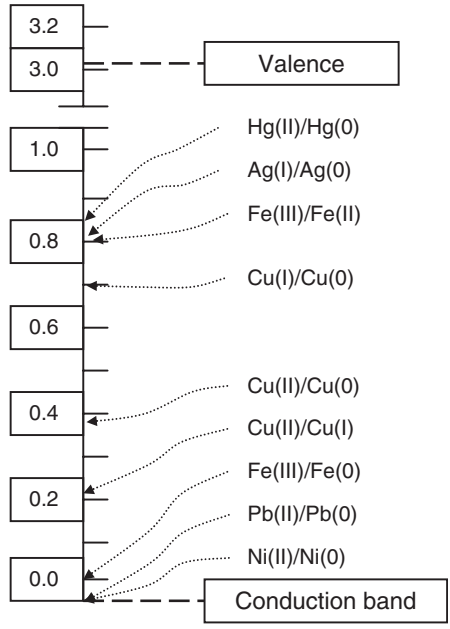

Figure 1 Reduction potential of different metal ions at pH 3 compared to TiO_2 conduction and valence bands (Chen and Ray, 2001).

In light of these findings, a new advantageous and characteristic of photocatalysis was discovered: the reduction of inorganic metal ions and the oxidation of organic molecules could be carried out simultaneously in a PC reactor. The photogenerated electron e^-_{cb} could help reduce the metallic ion while the photogenerated hole h^+_{vb} could promote the oxidation of an organic molecule. This fact, as will be discussed later, would reduce the recombination of the generated charges, thus increasing the energy efficiency of the system (Colon et al., 2001; Hufschmidt et al., 2002; Vamathevan et al., 2002).

It was also found that there exists a synergic effect in the organic oxidation and inorganic reduction. Some studies show that the presence of some metal ions can affect the rate of oxidation of organic molecules. For instance, the rate of oxidation of phenol can be affected by the presence of silver (Huang et al., 1996) and silver can also affect the oxidation of textile dyes (Sokmen and Ozkan, 2002). The presence of Cr(VI) affects the rate of oxidation of salicylic acid (Colon et al., 2001).

Likewise, the presence of organic molecules can accelerate or decelerate the rate of reduction of metal ions. The presence of a dye in the photoreduction of Cr(IV) increases the rate of reduction compared to when there is no dye present (Li Puma and Lock Yue, 1999).

With regard to the oxidation reactions of organic compounds, although there is still controversy over the actual oxidation mechanism, there is general consensus that hydroxyl $HO^{\bullet}$ radicals are the primary oxidizing species in a PC reaction. However, the oxidation of an organic molecule can proceed via $HO^{\bullet}_{ads}$-attack or h^{+}_{vb}-attack (Zertal et al., 2004). The prevailing mechanism greatly depends on the substrate and on the catalyst surface characteristics (Carraway et al., 1994; Yang et al., 2006). The steps that proceed via $HO^{\bullet}_{ads}$-attack, for instance, are significantly affected by the presence of a hydroxyl radical $HO^{\bullet}_{ads}$ scavenger (e.g., isopropanol), while the steps that follow the h^{+}_{vb}-attack remain unaltered. In some cases, it was possible to switch from h^{+}_{vb}-attack to $HO^{\bullet}_{ads}$-attack in the presence of ions such as F^{-} or SO_4^{2-} (Yang et al., 2006). In spite of these observations, it is still difficult to distinguish between these two mechanisms as both, in many cases, lead to the same reaction products (Grela et al., 1996; Carraway et al., 1994). The presence of hydroxylated compounds as reaction intermediates and the detection of hydroxyl radicals through electron spin resonance (ESR) technique lead to the conclusion that in many cases the oxidations are via $HO^{\bullet}_{ads}$-attack (Turchi and Ollis, 1989; 1990). Other studies also report the detection of hydroxyl radicals with various techniques such as spin trapping with electron paramagnetic resonance (EPR) (Riegel and Bolton, 1995) that support the $HO^{\bullet}_{ads}$-attack mechanism.

1.4. Iron (Fe) ions in photocatalytic processes

As shown above, some metals can be reduced in their oxidation states in a PC process. Ferric ions Fe^{3+}, for instance, can be reduced to ferrous ions Fe^{2+} with the photogenerated electron e^{-}_{cb} given that the reduction potential is 0.77 eV, which lies within the reduction potential of e^{-}_{cb}. Of the metals shown in Figure 1, Fe is the most benign and is actually needed for a proper human metabolism. Fe is also one of the most abundant metals in the earth only after aluminum. Moreover, it is also the fourth most abundant element in the earth's crust. The major iron ores are hematite (Fe_2O_3), magnetite (Fe_3O_4), limonite [FeO(OH)], and siderite ($FeCO_3$) (Cotton et al., 1999). Thus, because it is naturally present in large amounts and it possesses some PC properties, it represents an excellent candidate for the enhancement of the PC process. There are some interesting contributions confirming that the PC properties of iron can be exploited in photoreactions.

In this regard, Fe ions have been commonly used in advanced oxidation processes in what is known as the Fenton's reaction. This involves the reaction between hydrogen peroxide H_2O_2 and ferric (Fe^{3+}) and ferrous (Fe^{2+}) ions to produce hydroxyl radicals $HO^{\bullet}$ and perhydroxyl radical $HO^{\bullet}_2$. Fe^{3+} ions form a complex with H_2O_2 (see reaction (17) below). This complex further decomposes to produce Fe^{2+} ions and perhydroxyl radicals $HO^{\bullet}_2$ (reaction (18)). Fe^{2+} ions are then reoxidized to Fe^{3+} by reacting with

more H_2O_2 to produce a hydroxyl ion HO^- and a hydroxyl radical $HO^\bullet$ (reaction (1)) (Pignatello et al., 1999; Kavitha and Palanivelu, 2004; Poulopoulos and Philippopoulous, 2004).

$$H_2O_2 + Fe^{3+} \rightarrow Fe - OOH^{2+} + H^+ \quad (1)$$

$$Fe - OOH^{2+} \rightarrow Fe^{2+} + HO_2^\bullet \quad (2)$$

$$H_2O_2 + Fe^{2+} \rightarrow Fe^{3+} + HO^- + HO^\bullet \quad (3)$$

The above reactions (1–3) can occur in the dark or under near UV or visible light ($\lambda = 436$ nm) (Zepp et al., 1992). When the solution is irradiated, the rate of hydroxyl radical $HO^\bullet$ formation is accelerated by the decomposition of H_2O_2 with radiation of less than 360 nm (Pignatello et al., 1999). The decomposition of $Fe - OOH^{2+}$ is also accelerated with wavelengths lower than 313 nm (Cermenati et al., 1997; Domenech et al., 2004).

The perhydroxyl radicals $HO_2^\bullet$ can further react with either Fe^{2+} to produce more H_2O_2 (reaction (4)) or Fe^{3+} to produce molecular oxygen O_2 and a proton H^+ (reaction (5)).

$$HO_2^\bullet + Fe^{2+} + H^+ \rightarrow Fe^{3+} + H_2O_2 \quad (4)$$

$$HO_2^\bullet + Fe^{3+} \rightarrow Fe^{2+} + O_2 + H^+ \quad (5)$$

$$H_2O_2 + HO^\bullet \rightarrow HO_2^\bullet + H_2O \quad (6)$$

$$HO^\bullet + Fe^{2+} \rightarrow Fe^{3+} + HO^- \quad (7)$$

Additionally, reaction (6) can also take place in this system if H_2O_2 is in excess. Moreover, hydroxyl radicals can also be trapped by excess of ferrous ions (reaction (7)). Thus, despite the advantages such as commercial availability of the oxidant, no mass transfer problems, and formation of hydroxyl radicals from H_2O_2, this process presents several serious drawbacks. One of the most important one is that H_2O_2 has to be continuously added in controlled amounts as a source of hydroxyl radicals (Domenech et al., 2004).

Fe, on the other hand, has been used directly in PC processes as a dopant in semiconductors, in particular for TiO_2. The results seem to be somewhat contradictory nonetheless. These doped catalysts have been tested in the PC reactions of short-chain carboxylic acids such as maleic, formic, and oxalic acids, among others.

Some authors (Araña et al., 2001, 2002, 2003; Franch et al., 2005) have reported the activity of catalysts of TiO_2 doped with Fe in reactions with carboxylic acids such as maleic, formic, acetic, and acrylic acids. They found

that catalysts with 0.5 wt% of Fe prepared by incipient wetness impregnation yielded higher mineralization rate for both formic and maleic acids than the undoped TiO_2. However, for acetic and acrylic acids, all Fe-doped TiO_2 catalysts showed lower activities than the Fe-free TiO_2 samples. For formic and maleic acids, they observed that as the Fe wt% increased, the mineralization rate decreased.

With the sol-gel preparation method (Navío et al., 1996, 1999), however, all doped catalysts yielded lower activities than the untreated TiO_2. These authors showed that only those doped catalysts prepared through incipient wetness impregnation and low Fe% produced better results than the untreated TiO_2.

The doping procedures for both methods (wet impregnation and sol-gel) require elaborate steps of impregnation and calcination (at 773 K). Moreover, in the case of samples yielding better results and prepared via impregnation method, it was detected that deposited iron leaches out of the lattice of TiO_2 by forming photoactive complexes of the type $[Fe - Acid]^{n+}$ with the model reactants. This suggests that one has to be very cautious while preparing doped photocatalysts to prevent the metal from leaching out of the catalyst structure.

Another study on the use of Fe showed that the oxidation rate of acetaldehyde was improved with TiO_2 catalysts doped with Fe and Si synthesized by thermal plasma (Oh et al., 2003). A Fe content lower than 15% rendered higher activities than the untreated catalyst. The catalyst preparation technique involved a complex procedure using a plasma torch, with all this likely leading to an expensive photocatalyst of mild prospects for large-scale applications.

From the studies above, one can observe that the use of Fe has been somewhat limited and that there are still many areas to explore for better utilization of Fe in PC reactions. More specifically, there is a need for the development of new inexpensive techniques or procedures to increase the photocatalyst activity. These new procedures should make the process more efficient without the economic burden that photocatalyst doping brings about. Also, one can notice that most studies have focused on carboxylic acid species containing less than four carbons. It is of utmost importance to explore this area with more refractory molecules such as phenol and other hydroxylated aromatics to determine whether Fe can truly be applied to enhance the PC mineralization.

In this regard, the PC oxidation of phenol produces similar hydroxylated aromatics as reaction intermediates since the oxidation occurs via hydroxyl radical attack. These intermediates might be equally harmful than the parent species. Several authors report that during the oxidation of phenol, they identified various hydroxylated intermediates such as 1,2,3-trihydroxybenzene (1,2,3-THB), *ortho*- and *para*-dihydroxybenzene (*o*,*p*-DHB) (Al-Ekabi and Serpone, 1988), 1,2,4-THB and 1,4-benzoquinone (1,4-BQ)

(Trillas et al., 1992; Winterbottom et al., 1997), *p*-DHB, and 1,4-BQ (Leyva et al., 1998; Tseng and Huang, 1990). These intermediate species were detected in experiments performed over a wide range of conditions and in different reaction setups. Therefore, the formation and concentration of reaction intermediates greatly depend on the conditions at which the reaction takes place. The pH of the solution plays a key role in the formation of oxidation intermediates. Salaices et al. (2004), for instance, reported the formation of significant amounts of *p*- and *o*-DHB at a pH of 4, while the latter was not formed at pH of 7. Moreover, *o*-DHB was not detected when the catalyst was changed from Degussa to Hombikat UV-100. Also, 1,2,4-THB and 1,4-BQ were identified in most experiments with their concentrations not varying significantly from run to run.

Additionally to phenolic intermediates, upon the aromatic ring opening, a series of carboxylic acids can be formed. Maleic acid, for instance, has been detected in the oxidation of byphenyls (Bouquet-Somrani et al., 1996), 1,2,4-THB (Li et al., 1991a), 1,2-dimethoxybenzene (Pichat, 1997), and acid orange 7 (Stylidi et al., 2003). Similarly, muconic acid has been reported as an intermediate of byphenyls oxidation (Bouquet-Sormani et al., 1996), while succinic and malonic acids were identified in polycarboxylic benzoic acid oxidation (Assabane et al., 2000). It is therefore expected that these or similar acids be formed during phenol oxidation.

The presence of Fe ions in PC reactions could have an important effect on the formation and distribution of all reaction intermediates. The use of Fe ions in the PC oxidation of phenol as reaction enhancer may not only affect the rate of oxidation, but also promote different reaction pathways leading to changes in the intermediate species distribution or to the formation of new ones.

A complete identification and quantification of aromatics and carboxylic acids, during the oxidation of phenol for both unpromoted PC reaction (no iron present) and PC reaction coupled with Fe ions, will allow the formulation of a comprehensive reaction network for both systems and thus, a systematic comparison between them. Also, this will permit the development of a more detailed kinetic model to incorporate most of the oxidation intermediates for both systems and will definitely help determine the role of Fe ions in PC reactions.

Regarding the kinetic modeling, few contributions propose kinetic models for the PC oxidation of phenol and other aromatics (Chen and Ray, 1998, 1999; Li et al., 1999b; Wei and Wan 1992;), with kinetic models being based mainly on the initial rates of reaction only. Such models fail to account for the formation of the different reaction intermediates, which may play an important role in the overall mineralization rate. More recently, Salaices et al. (2004) developed a *series–parallel* kinetic model based on observable aromatic intermediates. This model was applied to a wide range of pH, phenol concentration, and catalyst type. In this model, however, some steps

were stated as hypothetical with no carboxylic acids being identified. To our knowledge, systematic studies dealing with all possible kinetic steps of PC oxidation of phenol and other hydroxylated aromatics with and without Fe ions have not been carried out.

1.5. Kinetic modeling

There is general consensus and evidence that PC reactions take place on the photocatalyst surface (Minero et al., 1992; Pellizetti, 1995). Several authors have studied the kinetics of pollutants degradation and found that the rate of reaction follows a Langmuir-Hinshelwood (LH)-type equation (Al-Ekabi et al., 1989; Okamoto et al., 1985; Turchi and Ollis, 1989, 1990). A LH equation type can be used as well for the degradation of phenol and its intermediates. In this regard, only a few studies have reported kinetic models for the oxidation of phenol and hydroxylated compounds (Li et al., 1999; Wei and Wan, 1992). Such kinetic models are based mainly on the initial reaction rates and fail to account for reaction intermediates that may play an important role in the kinetic expressions. In a more recent study, Salaices et al. (2004) developed a series–parallel kinetic reaction network for the photodegradation of phenol. This model involved LH equations for phenol and its major aromatic intermediates and was applied to various reaction pHs, different catalysts, and substrate concentrations with all conditions yielding good fitting of the model. Given the background provided by such study, phenol and other phenolic compounds are employed as model pollutants for establishing kinetics in the context of LH-type models.

1.6. Recent advances in CREC

CREC researchers have addressed recently the application of Fe cations as additives to enhance the performance of PC reactions employing inexpensive procedures. This was sought owing to the characteristic properties and behavior of Fe cations in a PC reaction. Phenol and similar aromatics were selected as model pollutants given their refractory nature in water treatment and health problems associated with their presence in drinking water.

In this respect, the effect of Fe cations on both the oxidation rate and complete mineralization rate of phenol and alike aromatic compounds was considered. Optimum conditions were reviewed to use Fe cations as reaction enhancers (henceforth PC reactions involving optimum Fe concentrations are called Fe-assisted PC reactions). This also involved the assessment of effect and mechanism of Fe ions on the PC reaction of phenol and other selected aromatic species. A systematic comparison between the kinetic reaction schemes for both unpromoted PC and Fe-assisted PC reactions for the selected model pollutants was also a primary emphasis. Last, the estimation of the enhancement through efficiency factor calculations was described.

Following this, efforts were devoted to the development of kinetic models to represent the PC oxidation of phenol. In this regard, models for the unpromoted PC reaction and a model for the Fe-assisted reaction are needed to account for the specific type of intermediates and their concentrations. This was necessary since Fe ions can alter the oxidation pathways yielding different amounts and various types of intermediates. For these studies, slurry-type PC reactors are the main experimental apparatus. While there is a considerable effort to find new PC reactors in which the catalyst is supported instead of being suspended to avoid catalyst loss or to ease its separation from the slurry, it is well established that slurry reactors provide more certainty of the photocatalyst loading used in a given experiment and the extent of its irradiation (Aguado et al., 2000; Guillard, 2003; Preis et al., 1997) and in general yield higher reaction rates (Mathews and McEvoy, 1992; Wyness et al., 1994). Hence, the slurry Photo-CREC and Photo-CREC Solar Simulator are considered in this chapter as the primary systems to study and understand the PC oxidation pathways.

2. EXPERIMENTAL METHODS USED IN CREC

2.1. Reaction setup

The main experimental setup used in CREC studies is shown in Figure 2. It is comprised of a slurry-annular PC reactor (1), a mixing tank (2), and a pump (3). The entire system operates in batch mode. The reacting media is

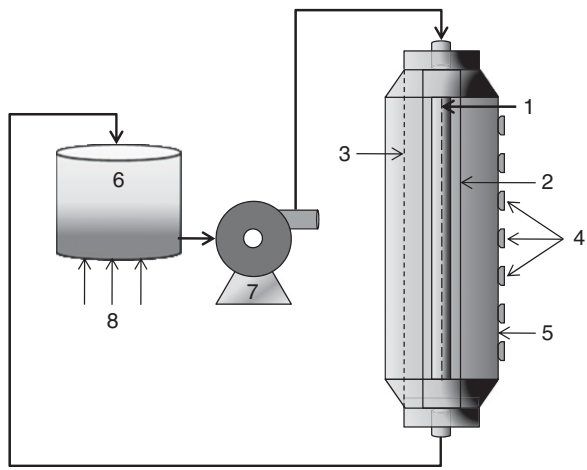

Figure 2 Schematic representation of the Photo-CREC Water-II Reactor: (1) MR or BL lamp, (2) replaceable 3.2-cm-diameter glass inner tube, (3) replaceable 5.6-cm-diameter glass inner tube, (4) fused-silica windows, (5) UV-opaque polyethylene outer cylinder, (6) stirred tank, (7) centrifugal pump, and (8) air injector.

first fed into the mixing tank and then pumped to the upper entrance of the reactor. After passing through the reactor annular section, the reacting media is pumped back to the mixing tank. A sampling port and an air supply are placed in the mixing tank. The Photo-CREC handles 6 L and has one lamp positioned in the center of the reactor. The lamp used in this reactor is a low-energy UV lamp. This reactor is equipped with fused-silica windows for absorbed irradiation measurements (de Lasa et al., 2005).

2.2. Reactants

The following reactants were used as received from suppliers without any further treatment: $FeSO_4$ $7H_2O$, phenol, TiO_2 P25 (Degussa), catechol, hydroquinone, 1,4-BQ, 1,2,4-benzentriol, fumaric acid, maleic acid, oxalic acid, and formic acid. Methyl viologen dichloride hydrate 98%, 4-chlorophenol 99%+, and Fe_2SO_3 H_2O were heated up for 2 h to 200°C and placed in a desiccator until they reached room temperature before preparing the solutions. H_2SO_4 was used in all experiments to control the pH of the reacting media.

2.3. Substrate analysis

2.3.1. Fe analysis

Fe content analyses were performed using a colorimetric technique as described in Karamanev et al. (2002).

2.3.2. Model pollutant analysis

The analyses of aromatic components were performed on a 1525 Binary Waters HPLC with a dual absorbance detector using a Symmetry C18 column and a mobile phase of methanol and water. Carboxylic acids analyses were performed using the same HPLC system with an Atlantis dC18 column and mobile phase. pH was monitored with a Corning 430 pH meter. For most experiments, the total organic carbon was also analyzed using a Shimadzu 5050 TOC analyzer equipped with a NDIR detector coupled with an autosampler ASI 5000.

The identification of both aromatic and carboxylic intermediates was performed comparing the retention times of model reactants with those of the reaction intermediates detected in the samples. Additionally, comparisons with spectra provided in catalogs from column manufacturers were made to corroborate the identification of reaction intermediates.

2.4. Catalyst elemental analysis: EDX and XPS

Samples for catalyst elemental analysis were prepared as follows: After taken from the continuous stirred tank (CST), they were let settle down overnight.

The supernatant was removed after 12 h of settling. The catalyst-rich solution was used for analysis. A few drops of this concentrate were placed over silicon films and the water was let to evaporate. Dried samples were then analyzed.

Selected samples from various experiments were analyzed in energy dispersive X-ray spectroscopy (EDX). These analyses were carried out on a Hitachi S-4500 field emission scanning electron microscopy equipped with an EDAX^{TM} Phoenix model EDX spectrometer. An electron beam of 15 kV was used. These samples were also analyzed in a Kratos Axis Ultra X-ray photoelectron spectroscopy (XPS).

2.5. Experiments in photo-CREC unit

The detailed experimental procedure for this study is explained elsewhere (Ortiz-Gomez et al., 2008). In general, a predefined amount of reactant was weighed. It was then added to a known volume of water, whose pH was adjusted with a H_2SO_4 solution. In the experiments with Fe ions, the Fe solution containing the desired amount of Fe (either as Fe^{3+} or Fe^{2+}) was premixed with TiO_2 in 100 mL for 30 min, then it was added to the previous mixture. H_2SO_4 solution was added to adjust the pH. The reactants were allowed to be in contact with the catalyst for 30 min or more before the UV lamp was turned on. During this period of time (dark period), the reacting media was pumped around the system. After this period, the lamp was turned on. All other operating conditions (air flowrate, reacting media flowrate, catalyst weight $-0.14\,g\,L^{-1}$, room temperature) were kept constant, except for the pH, which was not adjusted after the reaction started. Samples were taken at different time intervals to track the concentration of the reactants and intermediates.

3. Fe-ASSISTED PHOTOCATALYTIC MINERALIZATION OF PHENOL AND ITS INTERMEDIATES

In order to study the Fe-assisted PC mineralization of phenol, experiments were typically performed for the PC oxidation of phenol to determine the optimum pH at which the rate of oxidation was the highest possible in the reactor setup employed for this study. Then a series of tests were carried out to identify the aromatic and carboxylic intermediates of phenol oxidation at the optimum pH value. Subsequently, more tests with those aromatics identified as phenol oxidation intermediates were performed to unveil the intermediates produced during their corresponding PC oxidations and also to compare with the Fe-assisted PC reactions.

Once the kinetic reaction scheme for the unpromoted PC reaction of phenol and other aromatic species was determined, the next step was to

evaluate the influence of Fe cations on both the rate of oxidation and the rate of mineralization of phenol and similar hydroxylated aromatics.

A group of experiments was also performed to evaluate the extent of influence of Fe ions on the rate of oxidation of phenol. This new set was carried out at the optimum pH value determined in the previous runs. Once an optimum value of Fe ions was determined and the extent of influence assessed, more runs were performed using Fe ions from a different metallic complex to evaluate the effect of the oxidation state of the metal on the rate of oxidation (Ortiz-Gomez et al., 2008). Henceforth, the experiments with the optimum amount of Fe ions are referred to as Fe-assisted PC reactions.

Series of tests were also performed at optimum pH and optimum Fe ion concentrations to identify the oxidation intermediates for the Fe-assisted PC oxidation of phenol. Likewise, another series of experiments were performed to evaluate the effect of Fe ions on the rate of oxidation of those species identified as intermediates in the Fe-assisted PC oxidation of phenol.

All these data allowed the systematic comparison with the species detected and photoconversion rates observed in the unpromoted PC reactions.

3.1. Effect of Fe on the oxidation of phenol: optimum point and mechanism

A first set of experiments was aimed at evaluating the effect of Fe on the phenol oxidation rate at a concentration of 20 ppm C and at a pH of 3.2. The initial concentration of Fe cations was varied using different amounts of a solution containing Fe^{3+} ions.

It was found that the rate of phenol oxidation was significantly affected by the presence of ferric ions depending on their concentrations. This effect was a strong function of their initial concentrations, as shown in Figure 3. High Fe^{3+} ion concentrations considerably reduce the photo-oxidation rate revealing a negative effect of high ferric ion concentrations. To the contrary, Fe^{3+} ion concentrations below 10 ppm promote higher oxidation rates than those obtained in the unpromoted PC reaction. Moreover, as the concentration decreases below 10 ppm, the rate of phenol oxidation reaches a maximum value at 5 ppm of Fe^{3+} ions. Below this maximum, the rate decreases as well. Hence, it was determined that for the reaction conditions in Photo-CREC system, 5 ppm of ferric ions is the optimum Fe concentration. For additional information about the experiments with different iron concentrations, we advice the reader to refer to Ortiz-Gomez (2006).

The effect of 5 ppm of ferric ions is demonstrated for the oxidation of 50 ppm C in phenol, as shown in Figure 4. It can be observed that the addition of 5 ppm of Fe^{3+} ions promotes a higher oxidation rate than unpromoted PC reaction performed at pH 3.2.

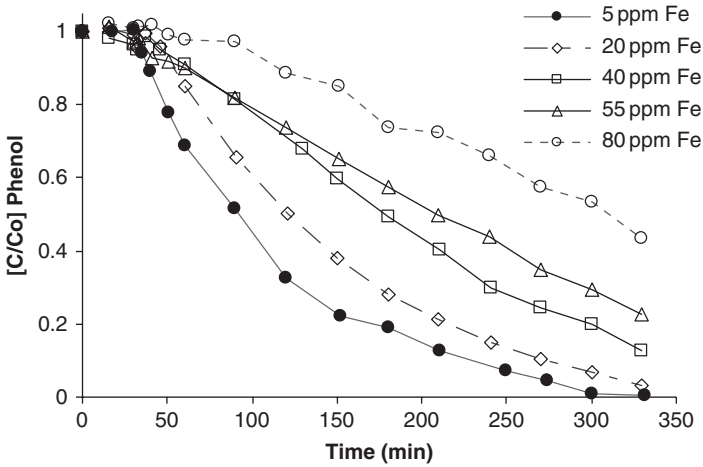

Figure 3 Influence of ferric ions on the rate of disappearance of phenol. 20 ppm C in phenol (Ortiz-Gomez et al., 2008).

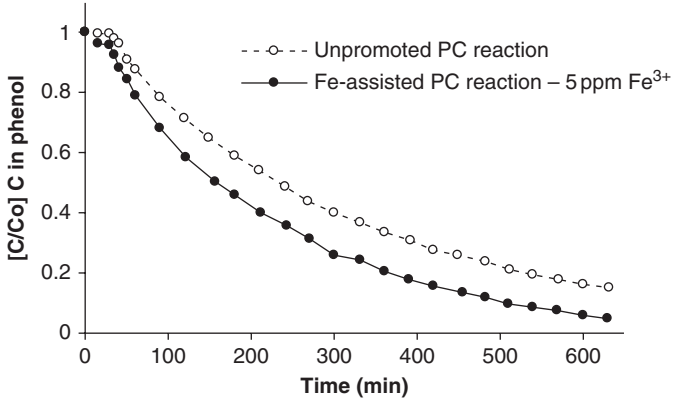

Figure 4 Influence of 5 ppm of ferric ions on the rate of oxidation of 50 ppm C in phenol (Ortiz-Gomez et al., 2008).

To determine the influence of the oxidation state of Fe ions on the rate of degradation of phenol, a new set of experiments using ferrous ions Fe^{2+} was carried out. It was found that regardless of the Fe oxidation state, be this state 3+ or 2+, adsorbed Fe onto TiO_2 promotes a higher oxidation rate than the unpromoted PC reaction. The concentration changes for the oxidation of 50 ppm C in phenol using Fe^{3+} and Fe^{2+} ions are shown in Figure 5a (5 ppm of Fe ions) and b (2 ppm of Fe ions). One can observe that photoconversion profiles are essentially identical and that the effect of the oxidation state of Fe, ferric or ferrous, yields the same results. Similar experiments were

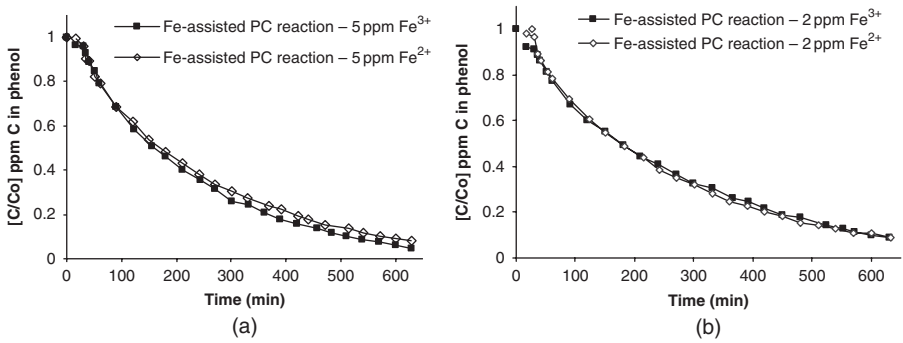

Figure 5 (a) Influence of ferric (Fe^{3+}) and ferrous (Fe^{2+}) on the oxidation rate of 50 ppm C in phenol. (b) Influence of 2 ppm of ferric and ferrous ions on the oxidation rate of 50 ppm C in phenol (Ortiz-Gomez et al., 2008).

carried out for different phenol concentrations with all cases showing and confirming the same behavior.

One can notice as well that the effect of Fe ions lasted throughout the reaction time. That is, its effect does not fade away with time. To the contrary, it has a major influence on the last stages of the PC conversion.

A number of studies using several metallic complexes have suggested that the enhancement in the oxidation rate by metals, such as Ag, Hg, and Cr, is due to the fact metal cations efficiently trap the photogenerated electrons e^-_{cb}, thus reducing the e^-_{cb}/h^+_{vb} recombination rate and leading to higher rates of hydroxyl radical formation by the hole h^+_{vb} (Colon et al., 2001; Oh et al., 2003). This mechanism seems appropriate for some metal cations; since once they are completely reduced to their lower oxidation state, their effect on the oxidation rate is diminished. Furthermore, in cases such as that of Ag and Cr they may bring the oxidation reaction to a halt by depositing the reduced cations on the catalyst surface and preventing the UV irradiation from reaching the catalyst surface (Chenthamarakshan and Rajeshwar, 2002; Colon et al., 2001; Navío et al., 1999).

The results of this study, however, reveal that Fe ions promote an enhancement through a different mechanism, as its change in the oxidation state does not have an influence on the oxidation reaction.

In the experiments with high concentrations of Fe^{3+} ions (shown in Figure 3), the change in the oxidation state of Fe^{3+} ions in the bulk of the liquid was also measured. In this regard, it was found that ferric ions are reduced to ferrous ions once the PC reaction was initiated. This cation reduction occurs in a relatively short time period compared with the phenol mineralization times. For instance, 20 ppm of ferric ions is completely reduced to ferrous ions in about 80 min while complete degradation of phenol is achieved in 330 min. This phenomenon is observed in all

experiments and for all tested Fe^{3+} concentrations. In every case, ferric ions are reduced to ferrous ions and remain in this state throughout the rest of the photoconversion reaction. Moreover, it is observed that the total Fe concentration is lower than the initial concentration. This confirms that Fe cations adsorb onto TiO_2 during the initial adsorption period in which the photocatalyst is first in contact with the Fe solution.

These results suggest that it is actually the Fe ions as Fe^{2+} ions that promote higher photoconversion reaction rates, as Fe^{3+} is quickly reduced to Fe^{2+}. Ferrous ions may be, however, quickly reoxidized to Fe^{3+} on the catalyst surface when an electron acceptor molecule, such as O_2, scavenges the e_{cb}^- forming a superoxide radical ($O_2^{-\bullet}$). This process appears to be similar to that reported for the platinization of TiO_2, where Pt reduces the recombination rate by transferring the electron to the O_2 molecule to form a superoxide radical (Hufschmidt et al., 2002).

It is important to point out that the optimum Fe concentration was determined from the total amount of iron added to the water system. Larger Fe concentrations yielded lower oxidation rates. This can be explained considering that higher Fe ion concentrations than 5 ppm might also increase the amount of iron remaining on the catalyst surface during the irradiation period. Those higher Fe concentrations on the surface might become "recombination centers" short-circuiting the photogenerated charges and thus, leading to higher recombination rates and higher inefficiencies. Araña et al. (2001, 2002) reported a similar effect on the Fe-doped catalysts, where those doped with high Fe content (2 wt%) yielded lower reaction rates than the ones with low Fe content (0.5 wt%). This was attributed to a similar phenomenon.

In a study with Fe-doped TiO_2, Araña et al. (2003) concluded that a catalyst containing 0.5 wt% of Fe showed an improvement in the oxidation of carboxylic acids. To prepare their Fe—TiO_2-doped catalysts, they followed a lengthy procedure that included a 48-h period of mixing of the solution containing the catalyst and Fe ions. After mixing, the catalyst was dried at 393 K for 24 h and then calcined at 773 K. The results obtained with those catalysts are similar to the results presented in this study, which were obtained with a much simpler and considerably less costly technique. This demonstrates then that a simple preimpregnation of the catalyst will render the same or better results than complex doping techniques.

Regarding iron addition as described above, one important consideration is the removal of the iron ions (Fe^{2+} or Fe^{3+}) in treated streams. These cation ions can easily be removed from treated water increasing the pH. This pH adjustment causes iron cation precipitation via the formation of iron hydroxide floccules. These floccules may entrap TiO_2-suspended particles facilitating both iron cations and TiO_2 removal from the treated water.

3.2. Fe-assisted mineralization of phenol and its intermediates

3.2.1. Oxidation of phenol: Fe-assisted PC reaction and its comparison with the unpromoted PC reaction

Given the findings reported in Ortiz-Gomez et al. (2008), all remaining experiments were developed with Fe^{3+} ions considering that the presence of iron as Fe^{2+} or Fe^{3+} is not significant and that both species lead to the same results.

Once the optimum amount of Fe ions was determined for the oxidation of 20 ppm C in phenol, new experiments were carried out to evaluate the effect of adding 5 ppm of ferric ions on different phenol concentrations (20, 30, 40, and 50 ppm C in phenol). This allows one to evaluate how Fe ions change the formation of reaction intermediates and, most importantly, how they influence the overall mineralization rate of phenol. These results are compared with those from unpromoted PC reaction.

In the experiments for the Fe-assisted PC reaction of phenol as a model reactant using 5 ppm of Fe^{3+}, various intermediates that included aromatics and carboxylic acids are identified. The major observed aromatic intermediates are *o*-DHB, *p*-DHB, and 1,4-BQ. The carboxylic acid intermediates are maleic acid (MeAc), fumaric acid (FuAc), oxalic acid (OxAc), and formic acid (FoAc). These are the same intermediaries detected in the unpromoted PC reaction of phenol (Ortiz-Gomez et al., 2007). The concentration profiles for the unpromoted PC oxidation of 30 ppm of phenol and its aromatic intermediates are shown in Figure 6a, while the concentration profiles for the Fe-assisted PC oxidation of 30 ppm C of phenol using 5 ppm of Fe^{3+} ions are shown in Figure 6b. It can be observed that in the presence of ferric ions, the formation of *o*-DHB is favored whereas that of *p*-DHB is suppressed. The increase in concentration of *o*-DHB is around the same magnitude of the decrease in *p*-DHB concentration. More detailed comparisons between the intermediates for both systems are presented in Figures 7 and 8.

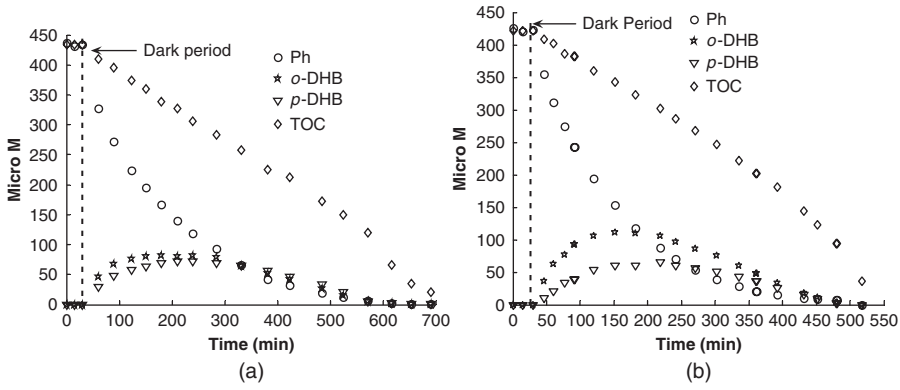

Figure 6 Concentration profiles for the (a) unpromoted PC oxidation of 30 ppm C in phenol and (b) Fe-assisted PC oxidation of 30 ppm C in phenol using 5 ppm Fe^{3+} ions (Ortiz-Gomez et al., 2008).

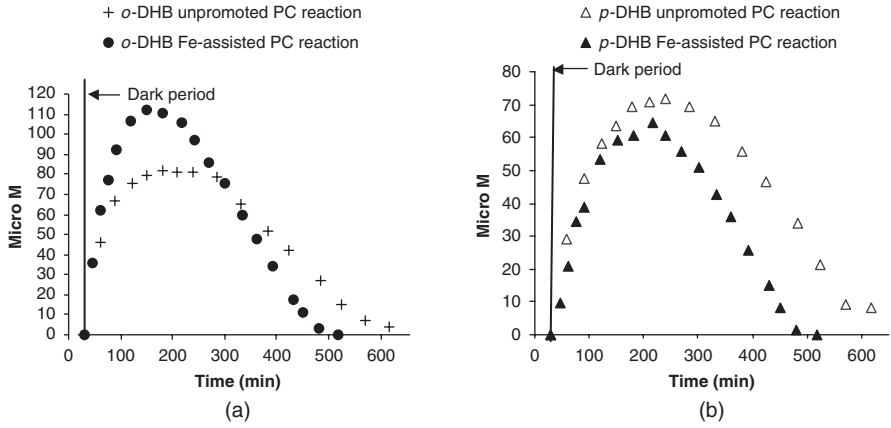

Figure 7 (a) *o*-DHB concentration profiles for both unpromoted PC reaction (30 ppm C in phenol) and Fe-assisted PC (30 ppm C in phenol + 5 ppm Fe^{3+} ions). (b) *p*-DHB concentration profiles for both PC reaction (30 ppm C in phenol) and Fe-assisted PC (30 ppm C in phenol + 5 ppm Fe^{3+} ions) (Ortiz-Gomez et al., 2008).

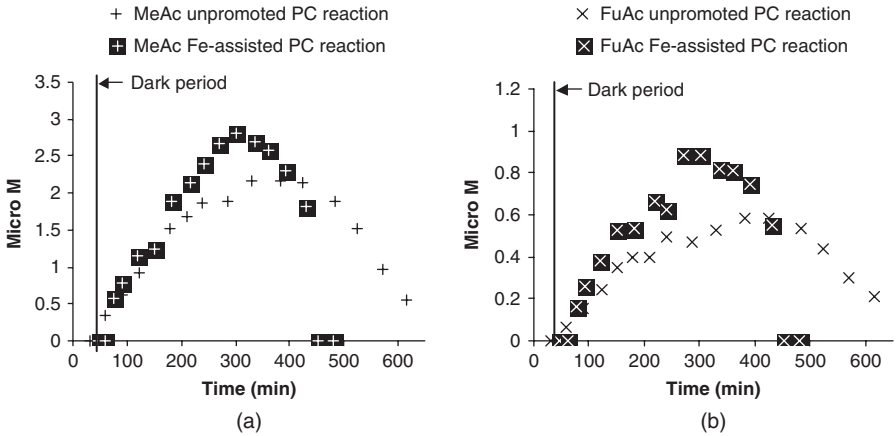

Figure 8 (a) MeAc concentration profiles for both unpromoted PC reaction (30 ppm C in phenol) and Fe-assisted PC (30 ppm C in phenol + 5 ppm Fe^{3+} ions). (b) FuAc concentration profiles for both PC reaction (30 ppm C in phenol) and Fe-assisted PC (30 ppm C in phenol + 5 ppm Fe^{3+} ions) (Ortiz-Gomez et al., 2008).

As shown in Figure 8a and b, the concentrations of carboxylic acids are also influenced by the presence of Fe^{3+} ions. For the Fe-assisted PC reaction, MeAc and FuAc concentrations slightly supersede the concentration for the unpromoted PC runs in the middle of the experiment and decrease more rapidly later. Similar trends were observed for OxAc and FoAc.

An additional effect, which is the most important of all the phenomena observed in these experiments, is the effect the Fe^{3+} ions observe on the overall mineralization rate of phenol. The Fe^{3+} not only enhances the rate of oxidation of phenol and changes the formation of its oxidation intermediates but also accelerates the rate of its overall mineralization. Figure 9a and b compare the TOC profiles for the oxidation of 20 and 30 ppm C of phenol in both unpromoted PC and Fe-assisted PC systems. It can be seen that during the Fe-assisted PC reaction, the overall mineralization of phenol is faster than that for the unpromoted PC reaction. One can also observe that for both cases, during the first part of the reaction time, the two profiles follow a similar trend. The TOC profile in the Fe-assisted PC systems, however, drops off faster than that in the PC system. More importantly, one can notice that in the last part of the reaction period, there is a considerable change on the slope of the TOC profile in the Fe-assisted PC reactions.

In this respect, the overall mineralization rate of phenol has often been approximated with a zero-order reaction rate (Salaices et al., 2004) as it follows a fairly straight line. For the Fe-assisted PC reaction, however, this approximation cannot be applied given the sharp change of slope in the last part of the photoconversion reaction. Thus, a more complex kinetic rate equation needs to be developed to account for this behavior.

From the results above, it can be observed that as in the unpromoted PC oxidation, in the Fe-assisted PC oxidation of phenol all aromatic intermediates are detected in small amounts from the time when the photoreaction is initiated. One can notice as well that there is a rapid reduction in the TOC

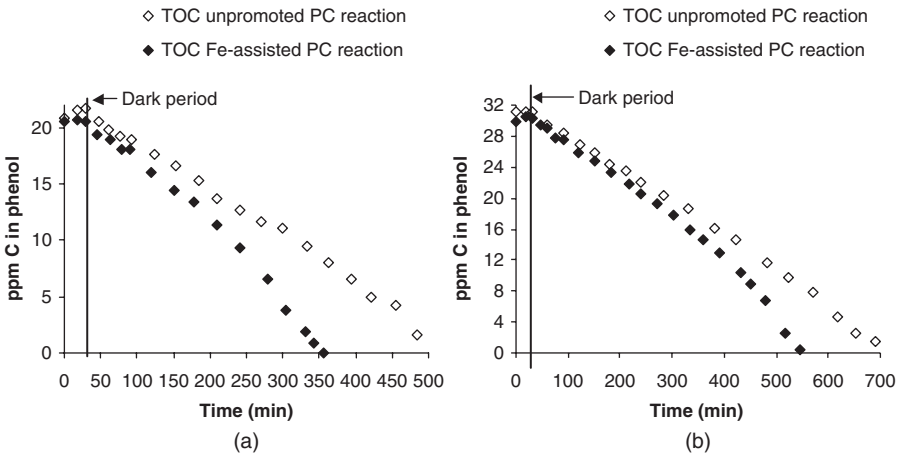

Figure 9 (a) TOC profiles for both unpromoted PC reaction (20 ppm C in phenol) and Fe-assisted PC reaction (20 ppm C in phenol + 5 ppm Fe^{3+} ions). (b) TOC profiles for both PC reaction (30 ppm C in phenol) and Fe-assisted PC reaction (30 ppm C in phenol + 5 ppm Fe^{3+} ions) (Ortiz-Gomez et al., 2008).

content from the early stages of the reaction, a phenomenon also observed in the unpromoted PC reaction. This can be equally attributed to a complete mineralization. As observed from the carboxylic acid profiles, they are also detected in the system once the lamp is turned on. Therefore, it can be concluded that in Fe-assisted PC reaction hydroxyl radicals oxidize phenol in a similar fashion but at a different rate than in the unpromoted PC oxidation. Phenol is simultaneously hydroxylated into *o*-DHB, *p*-DHB, and carboxylic acids and mineralized into CO_2. The aromatic intermediates can be further oxidized into carboxylic acids and CO_2. The carboxylic acids can be formed from the oxidation of all aromatics. Hence, the same concept of nonuniform distribution of hydroxyl radicals over TiO_2 surface leading to different degrees of oxidation can help explain the observed phenomena, with phenol having aromatic ring cleavage and formation of carboxylic acids and CO_2 as soon as the photoreaction is commenced.

Thus, considering the Fe-assisted PC conversion of phenol, the observable effect is that phenol produces many intermediate species from the start of the reaction regardless of the pathways involved in the production of such intermediates. It can thus be concluded that the Fe-assisted PC oxidation of phenol can be equally represented with a series–parallel reaction scheme, as it was for the unpromoted PC reaction. All the steps described above are summarized in Figure 10, a reaction scheme based on observable species. It must be emphasized that although the reaction network describes both unpromoted PC and Fe-assisted PC reactions, the values of the kinetic constants will be different for both systems.

3.2.2. Oxidation of *ortho*-dihydroxybenzene: Fe-assisted PC reaction and its comparison with the unpromoted PC reaction

Separate series of experiments were performed using *o*-DHB as model reactant to understand its behavior in the Fe-assisted reaction. In this case, in the Fe-assisted PC oxidation of *o*-DBH using 5 ppm Fe^{3+}, the only

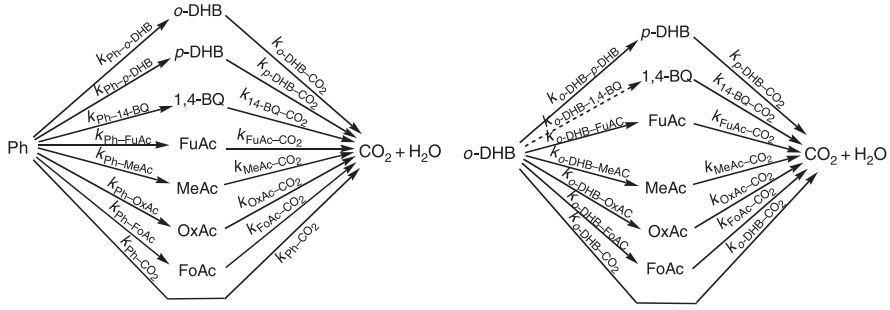

Figure 10 Series–parallel reaction scheme for oxidation of (a) phenol and (b) *o*-DHB involving all detected species. This applies to unpromoted PC and Fe-assisted PC reactions (Ortiz-Gomez et al., 2008).

aromatic observed was *p*-DHB. The same carboxylic acids in the unpromoted PC reaction were identified: FuAc, MeAc, FoAc, and OxAc.

It is shown that for *o*-DHB PC oxidation, the addition of 5 ppm Fe^{3+} ions also promotes an important improvement on the PC oxidation rate with respect to the unpromoted PC reaction, 1,4-BQ.

All observations lead to the conclusion that the oxidation of *o*-DHB follows a similar pattern than phenol oxidation in both unpromoted PC and Fe-assisted PC with all intermediates, aromatic species, and carboxylic acids being detected as soon as the photoreaction is initiated. This shows that some of the *o*-DHB molecules are quickly oxidized to CO_2, as suggested by the early decrease in TOC. Likewise, some *o*-DHB molecules are partially oxidized to carboxylic acids. These results demonstrate that the oxidation of *o*-DHB can also be represented with a series–parallel reaction scheme.

3.2.3. Oxidation of *para*-dihydroxybenzene and 1,4-benzoquinone: Fe-assisted PC reaction and its comparison with the unpromoted PC reaction

The next set of experiments involved the Fe-assisted PC oxidation of *p*-DHB and 1,4-BQ as the model pollutants. In these cases, similar patterns were observed leading to the conclusion that these two compounds behave in a similar way to phenol and *o*-DHB with both exhibiting a series–parallel reaction scheme (Ortiz-Gomez et al., 2008)

3.2.4. Overall refined series–parallel reaction mechanism for PC and Fe-assisted PC reaction

Each of the series–parallel reaction schemes presented in the previous sections for the Fe-assisted oxidations of phenol, *o*-DHB, *p*-DHB, and 1,4-BQ, were established considering the chemical species detected in the bulk of the water solution. Given that *o*-DHB, *p*-DHB, and 1,4-BQ are intermediates in the Fe-assisted PC oxidation of phenol, an overall reaction scheme for the Fe-assisted PC oxidation of phenol can be formulated. This overall reaction network incorporates all the detected intermediaries.

The underlying assumption in this reaction scheme is that all chemical species behave the same as a model pollutant or as an intermediate. To exemplify, *o*-DHB is an intermediate in the Fe-assisted oxidation of phenol and when used as a model reactant, *o*-DHB forms *p*-DHB. It is hypothesized therefore that *o*-DHB as an intermediate in phenol Fe-assisted PC conversion forms *p*-DHB. Hence, the same assumptions for the development of the overall reaction scheme in the unpromoted PC reaction are considered for the Fe-assisted PC system.

The overall reaction network for the oxidation of phenol for the Fe-assisted PC reaction is depicted in Figure 11. The main differences with the unpromoted PC reaction scheme are highlighted with dashed arrows.

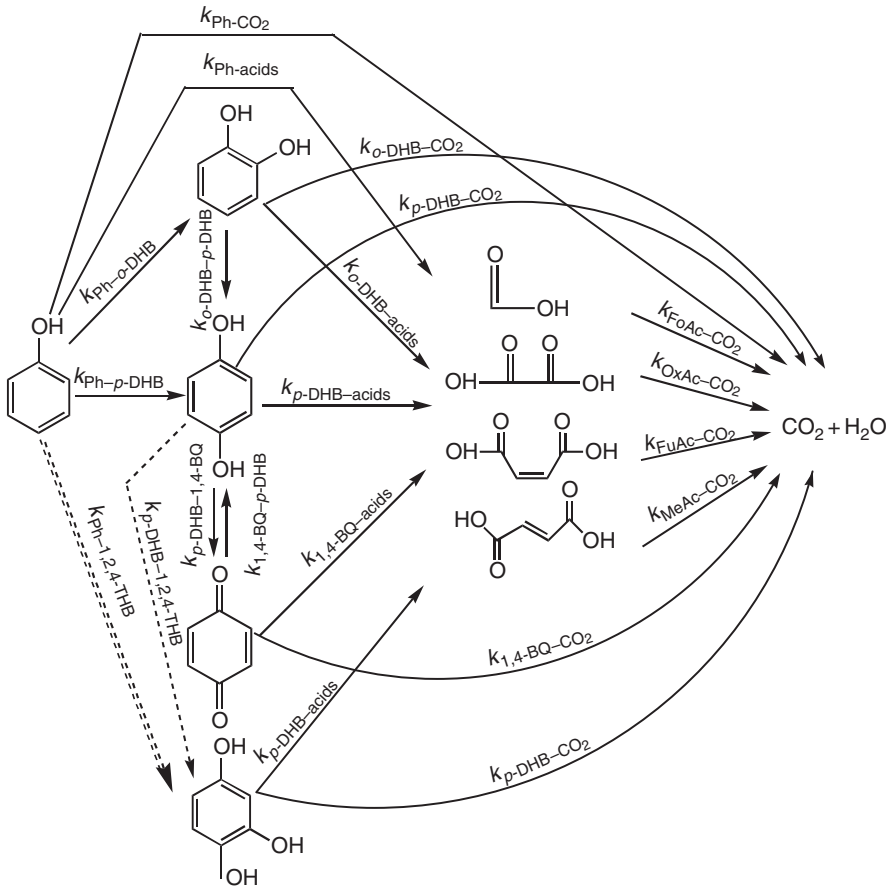

Figure 11 Detailed series–parallel reaction scheme for the unpromoted PC and Fe-assisted PC oxidation of phenol. Broken arrow applies only to PC reaction. Double broken arrow is established as a possible kinetic step not observed at experimental conditions for the reaction (Ortiz-Gomez et al., 2008).

A similar diagram was presented in a previous study for the unpromoted PC oxidation of phenol (Salaices et al., 2004). The reaction scheme introduced in this chapter incorporates all carboxylic acids detected in the oxidations of the various aromatic species, as well as the existing relationships among the intermediate species. A very important fact is that this newly developed reaction network describes the Fe-assisted PC oxidation of phenol as well as the unpromoted PC reaction. One important difference between the reaction scheme for the unpromoted PC reaction and that of the Fe-assisted PC reaction is the step relating the formation of 1,2,4-THB from

p-DHB. The 1,2,4-THB was not detected in any of the Fe-assisted runs, and this step is represented in Figure 11 with a broken arrow. All other steps apply to both unpromoted PC and Fe-assisted reactions alike.

The proposed reaction scheme encompasses a series of new contributions over those presented in previous studies. These include the following:

(a) the consideration that both unpromoted PC and Fe-assisted PC oxidation of phenol lead to the formation of the same aromatics *o*-DHB, *p*-DHB, and 1,4-BQ, and the same carboxylic acids FuAc, MeAc, OxAc, and FoAc, as reaction intermediates;
(b) the observation that both the unpromoted PC and the Fe-assisted PC oxidation of the three aromatic intermediates (*o*-DHB, *p*-DHB, and 1,4-BQ) produce the same aromatic and carboxylic intermediates, except for *p*-DH that in the Fe-assisted PC reaction no 1,2,4-THB is detected;
(c) the finding that in the oxidation of *o*-DHB, the *p*-DHB is formed as an intermediate in small amounts, being the only detected aromatic intermediary;
(d) the observation that the 1,4-BQ is reduced at a high rate to form *p*-DHB as soon as the catalyst is irradiated. Although the reaction *p*-DHB $\Leftrightarrow$ 1,4-BQ is a reversible reaction, the formation of *p*-DHB is more favorable during the PC reaction. The same behavior is observed in both unpromoted PC and Fe-assisted PC reactions;
(e) the finding that 1,2,4-THB formation from phenol can be presented as a possible step, in agreement with a series–parallel scheme for the unpromoted PC oxidation of *p*-DHB;
(f) the postulate that the reaction step relating the 1,4-BQ formation directly from phenol can be traced to the conversion of *p*-DHB.
(g) regarding the formation of 1,2,4-THB in the unpromoted PC oxidation of *p*-DHB, it was observed that during the unpromoted PC oxidation of 1,2,4-THB as a model pollutant (results not shown here), its reaction rate was very fast compared with the oxidation of the other aromatics. Moreover, the Fe-assisted PC reaction of 1,2,4-THB was even faster than the unpromoted PC reaction. Thus, it can be expected that if 1,2,4-THB is formed in the Fe-assisted oxidation of *p*-DHB, it will disappear very quickly as well, keeping its concentration below the detectable limit.

4. KINETIC MODELING: UNPROMOTED PC OXIDATION AND Fe-ASSISTED PC OXIDATION OF PHENOL

4.1. Overall kinetic model

For the overall series–parallel reaction scheme, a set of differential equations can be developed to describe the rates of formation and disappearance of phenol and all its aromatic and carboxylic intermediates. It is well known

that PC reactions occur on the catalyst surface, therefore the rates of formation and disappearance of all components can be modeled using a LH-type rate equation, which takes into account the adsorption of the reactants on the catalyst surface as well as the reaction kinetics. The general form of a LH equation for this system is given by (Ollis et al., 1989)

$$r_i = \frac{k_i^k K_i^A C_i}{1 + \sum_{j=1}^{n} K_j^A C_j} \tag{8}$$

where r_i is the rate of reaction of component i in mol/(g_{cat} min), k_i^k is the kinetic constant for component i in mol/(g_{cat} min), K_i^A is the adsorption constant for component i in $L\,M^{-1}$. j is a subscript to denote each component in the denominator term while n is the number of chemical species. In addition, considering that the system in which the experiments were carried out operates in batch mode, a balance equation for each component i can be expressed as follows:

$$\frac{V dC_i}{W dt} = r_i \tag{9}$$

where V is the volume of the reactor in L, W is the weight of the catalyst in g, and t is the time in minutes. By combining Equations (8) and (9), the general form for the rates of reaction for each chemical species is obtained:

$$\frac{dC_i}{dt} = \frac{\frac{W}{V} k_i^k K_i^A C_i}{1 + \sum_{j=1}^{n} K_j^A C_j} \tag{10}$$

Let $k_i = \frac{W}{V} k_i^k K_i^A$, then Equation (10) can be simplified to

$$\frac{dC_i}{dt} = \frac{k_i C_i}{1 + \sum_{j=1}^{n} K_j^A C_j} \tag{11}$$

All rate constants in Equation (11) represent apparent constants. The intrinsic kinetic constant can be calculated using the following relationship (Salaices et al., 2004; Wolfrum and Turchi, 1992):

$$k_i^I = \frac{V_{CST} + V_{PFR}}{V_{PFR}} \tag{12}$$

Thus, by developing one equation with the form of Equation (11) for each component, one can obtain a set of differential equations to represent the PC oxidation of phenol. One should notice, however, that in the following

kinetic modeling, the 1,2,4-THB intermediate considered in Figure 11 was omitted in the analysis given that it was not detected directly in the oxidation of phenol. As a result, the 1,2,4-THB formation and consumption steps are not accounted for in the following rate equations.

First, for phenol the rate of reaction is given by

$$\frac{dC_{Ph}}{dt} = \frac{-(k_{Ph\rightarrow Ac} + k_{Ph\rightarrow o\text{-DHB}} + k_{Ph\rightarrow p\text{-DHB}} + k_{Ph\rightarrow CO_2})C_{Ph}}{1 + K^{A}_{Ph}C_{Ph} + K^{A}_{o\text{-DHB}}C_{o\text{-DHB}} + K^{A}_{p\text{-DHB}}C_{p\text{-DHB}} + K^{A}_{14-BQ}C_{14-BQ} + K^{A}_{Ac}C_{Ac}} \tag{13}$$

where $k_{Ph\rightarrow Ac}$ is a lumped kinetic constant that includes all the kinetic constants for the production of acids from phenol and is given by

$$k_{Ph\rightarrow Ac} = k_{Ph\rightarrow FoAc} + k_{Ph\rightarrow OxAc} + k_{Ph\rightarrow MeAc} + k_{Ph\rightarrow FuAc} \tag{14}$$

and the last term in the denominator involving all the adsorption terms for all carboxylic acids, which is defined as

$$K^{A}_{Ac}C_{Ac} = K^{A}_{FoAc}C_{FoAc} + K^{A}_{OxAc}C_{OxAc} + K^{A}_{MeAc}C_{MeAc} + K^{A}_{FuAc}C_{FuAc} \tag{15}$$

Similar equations can be written for each intermediate as described in Ortiz-Gomez et al. (2008).

4.2. Parameter estimation

The validation of the proposed kinetic model can be done through the estimation of parameters in the equations by fitting the experimental data. The mathematical model with the best parameter estimates can be used to predict the behavior of a system where that model is assumed to describe the process. Since the Ordinary Differential Equation (ODE) system describing the process cannot be solved analytically, the problem is to determine the parameters using a different algorithm that calls for the iterative integration of the ODEs set and the minimization of an objective function (Englezos and Kalogerakis, 2001). For additional details, please refer to Ortiz-Gomez et al. (2007).

4.2.1. Constrained relationships for the estimation of parameters

The analysis of the set of equations reveals that there are two important relationships that must be established before all parameters can be estimated simultaneously. One of them is between $k_{o\text{-DHB}\rightarrow p\text{-DHB}}$ and $(k_{o\text{-DHB}\rightarrow Ac} + k_{o\text{-DHB}\rightarrow CO_2})$ and the second one between $k_{14\text{-BQ}\rightarrow p\text{-DHB}}$ and $k_{p\text{-DHB}\rightarrow 14-BQ}$, given that these relationships might affect the parameter estimation if they are not clearly defined beforehand. Bearing in mind that the estimation of parameters is based on the minimization of an objective function, the minimization can lead to unfeasible solutions or solutions that

do not fully represent the real phenomena if these relationships are not constrained. For instance, the solver may converge to a solution where $k_{o\text{-DHB}\rightarrow p\text{-DHB}}$ is much larger than $(k_{o\text{-DHB}\rightarrow \text{Ac}} + k_{o\text{-DHB}\rightarrow \text{CO}_2})$ and still be a minimum of the objective function. However, from the unpromoted *o*-DHB reaction, it is quite apparent that *o*-DHB forms *p*-DHB in low amounts with most of *o*-DHB being converted into acids and CO_2. Thus, a very large $k_{o\text{-DHB}\rightarrow p\text{-DHB}}$ would not be an acceptable solution despite the fact that it might lead to a lower value of the objective function. The estimation of these relationships is shown elsewhere (Ortiz-Gomez et al., 2008).

The values of the estimated parameters and their confidence intervals (CI) are presented in Table 1. From these results, a ratio R of $k_{o\text{-DHB}\rightarrow p\text{-DHB}}$ to $k_{o\text{-DHB}\rightarrow \text{CO}_2}$ can be established and used to constrain the estimation of parameters in the complete reaction system.

Likewise, the values of the estimated parameters for the second constraint are reported in Table 2. These results show that the reverse reaction kinetic constant $k_{14\text{-BQ}\rightarrow p\text{-DHB}}$ is extremely large compared to forward reaction kinetic constant, $k_{p\text{-DHB}\rightarrow 14\text{-BQ}}$. Similar results were obtained for different 1,4-BQ and *p*-DHB concentrations. Even more, the estimated value is much lower than its CI. Thus, this kinetic constant is statistically insignificant and should be dropped from the kinetic model altogether. Hence, it can be assumed that in all cases the production of 1,4-BQ from *p*-DHB will be extremely small. Only in cases where there is some 1,4-BQ at the beginning of the reaction, it will immediately convert to *p*-DHB once the PC reaction is initiated, and the step considering the formation of *p*-DHB from 1,4-BQ has to be included. However, if the concentration of 1,4-BQ at the beginning of the reaction is negligible, all terms involving 1,4-BQ concentrations and their related constants can be safely omitted from the kinetic models since 1,4-BQ is not formed in significant amounts.

Table 1 Estimated parameters for the unpromoted PC and Fe-assisted PC oxidation of *ortho*-dihydroxybenzene (20 ppm C in *o*-DHB)

	Unpromoted PC oxidation		Fe-assisted PC oxidation	
	Estimate	CI	Estimate	CI
$k_{o\text{-DHB}\rightarrow \text{CO}_2}$ (1/min)	6.19e-04	5.0e-04	1.03e-03	6.5488e-04
$k_{o\text{-DHB}\rightarrow p\text{-DHB}}$ (1/min)	1.49e-04	1.0e-04	1.2270e-04	8.5995e-05
$K^{\text{A}}_{o\text{-DHB}}, K^{\text{A}}_{p\text{-DHB}}$ (1/μM)	5.22e-02	4.28e-2	5.57e-02	3.93e-2
$R = {k_{o\text{-DHB}\rightarrow \text{CO}_2}}/{k_{o\text{-DHB}\rightarrow p\text{-DHB}}}$	4.15		8.39	

Table 2 Estimated parameters for both unpromoted PC and Fe-assisted PC oxidations of 1,4-benzoquinone

	Unpromoted PC oxidation		Fe-assisted PC oxidation	
	Estimate	CI	Estimate	CI
$k_{p\text{-DHB}\rightarrow 1,4\text{-BQ}}$ (1/min)	2.34e-14	1.01e-04	2.33e-14	1.11e-04
$k_{14\text{-BQ}\rightarrow p\text{-DHB}}$ (1/min)	2.70e-03	1.20e-03	2.70e-03	1.30e-03
$k_{p\text{-DHB}\rightarrow CO_2}$ (1/min)	1.41e-04	1.00e-05	2.51e-04	1.00e-04
$k_{14\text{-BQ}\rightarrow CO_2}$ (1/min)	1.52e-04	2.00e-04	1.32e-04	2.01e-04
$K^{A}_{14\text{-BQ}}, K^{A}_{p\text{-DHB}}$ (1/μM)	3.20e-03	3.1e-03	4.9e-03	4.1e-03

Kinetic model #1 (KM#1): aromatics only The first proposed model considers that those aromatic intermediates produced in small amounts can be neglected and that all remaining aromatics are converted directly into CO_2 and water (e.g., formation of carboxylic acids is neglected). A schematic representation of this reaction network is given in Figure 12.

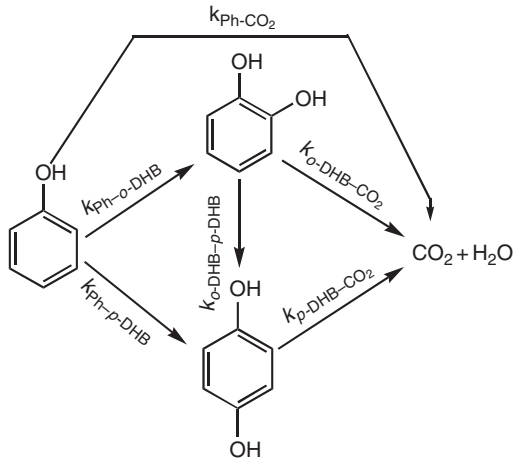

Figure 12 Schematic representation of reaction network for kinetic model #1 (KM#1) (Ortiz-Gomez et al., 2008).

This proposed model assumes the following:

(a) The concentration and rate constants for 1,4-BQ, 1,2,4-THB, and all carboxylic acids are neglected.
(b) There is an immediate conversion of phenol to CO_2, as demonstrated from the TOC profile, thus the constant $k_{Ph\rightarrow CO_2}$ is retained.
(c) The ratio R is included in the model to constrain the ratio of *o*-DHB producing *p*-DHB and CO_2.

The resulting differential equations are as follows

$$\frac{dC_{Ph}}{dt} = \frac{-(k_{Ph\rightarrow CO_2} + k_{Ph\rightarrow o\text{-DHB}} + k_{Ph\rightarrow p\text{-DHB}})C_{Ph}}{1 + K^A_{Ph}C_{Ph} + K^A_{o\text{-DHB}}C_{o\text{-DHB}} + K^A_{p\text{-DHB}}C_{p\text{-DHB}}} \tag{16}$$

$$\frac{dC_{o\text{-DHB}}}{dt} = \frac{k_{Ph\rightarrow o\text{-DHB}}C_{Ph} - \left[\left(\frac{k_{o\text{-DHB}\rightarrow p\text{-DHB}}}{R} + k_{o\text{-DHB}\rightarrow CO_2}\right)C_{o\text{-DHB}}\right]}{1 + K^A_{Ph}C_{Ph} + K^A_{o\text{-DHB}}C_{o\text{-DHB}} + K^A_{p\text{-DHB}}C_{p\text{-DHB}}} \tag{17}$$

$$\frac{dC_{p\text{-DHB}}}{dt} = \frac{k_{Ph\rightarrow p\text{-DHB}}C_{Ph} + \frac{k_{o\text{-DHB}\rightarrow p\text{-DHB}}}{R}C_{o\text{-DHB}} - k_{p\text{-DHB}\rightarrow CO_2}C_{p\text{-DHB}}}{1 + K^A_{Ph}C_{Ph} + K^A_{o\text{-DHB}}C_{o\text{-DHB}} + K^A_{p\text{-DHB}}C_{p\text{-DHB}}} \tag{18}$$

The results for the estimation of parameters using the data for three different concentrations (20, 30, and 40 ppm C in phenol) are shown in

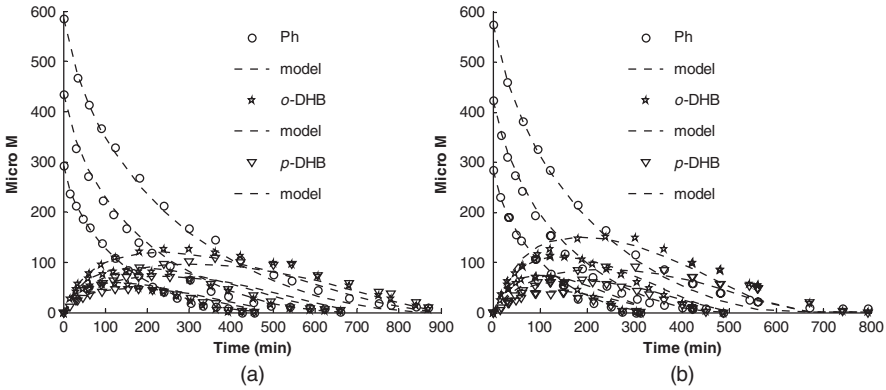

Figure 13 Experimental and predicted profiles of phenol, *ortho*-dihydroxybenzene, and *para*-dihydroxybenzene using KM#1 for (a) unpromoted PC oxidation and (b) Fe-assisted PC oxidation. Simultaneous parameter evaluation of 20, 30, and 40 ppm C in phenol (Ortiz-Gomez et al., 2008).

Table 3 Estimated parameters with KM#1 tcqazIn spite of these observations, it ation of phenol

	Unpromoted PC oxidation		Fe-assisted PC oxidation	
	Estimate	CI	Estimate	CI
$k_{Ph\rightarrow CO_2}$ (1/min)	1.14e-04	1.01e-04	1.15e-04	1.05e-04
$k_{Ph\rightarrow o\text{-DHB}}$ (1/min)	3.90e-04	2.46e-04	6.75e-04	5.66e-04
$k_{Ph\rightarrow p\text{-DHB}}$ (1/min)	2.49e-04	1.58e-04	2.98e-04	2.54e-04
$k_{o\text{-DHB}\rightarrow CO_2}$ (1/min)	5.03e-04	3.16e-04	6.97e-04	5.78e-04
$k_{p\text{-DHB}\rightarrow CO_2}$(1/min)	5.39e-04	3.31e-04	8.02e-04	6.62e-04
K^{A}_{Ph}(1/μM)	1.03e-02	8.00e-03	1.26e-02	1.02e-02
$K^{A}_{o\text{-DHB}}, K^{A}_{p\text{-DHB}}$ (1/μM)	3.78e-02	2.82e-02	3.78e-02	3.370e-02

Simultaneous parameter evaluation for 20, 30, and 40 ppm C in phenol.

Figure 13. Note that this model provides a good fit of the experimental data for both systems. The estimated rate parameters and their corresponding CI for this case are given in Table 3. This was done with the additional assumption that the adsorption constants for *o*-DHB and *p*-DHB are equal.

A comparison between the kinetic parameters obtained for both unpromoted PC and Fe-assisted PC is shown in Figure 14 (they are displayed in the same order as shown in the tables). One can observe that for the simultaneous concentrations of 20, 30, and 40 ppm C in phenol, the estimates obtained for the Fe-assisted PC oxidation are also higher than those estimated for the unpromoted PC reaction. This comparison allows to corroborate the model adequacy by producing estimates consistent with the experimental observations. That is, kinetic parameters in the Fe-assisted PC oxidation must be larger than in the unpromoted PC reaction.

Kinetic Model #2 (KM#2): lumped acids and CO_2 production The kinetic model #1 considers only the oxidation of the major aromatic intermediates. As shown in the previous section, when most of the major intermediates have been depleted, there is still a substantial concentration of other remaining organic intermediates, as the TOC profile indicates. Therefore, it is of particular interest to calculate and predict the total mineralization times. Also, with TOC measurements, it is possible to approximate the amount of CO_2 produced in the course of the reaction. In this new series–parallel model, the formation and disappearance of carboxylic acids as well as the production of CO_2 has been incorporated.

The representation of the experimental data with this new approach allows one to infer important information that can be applied for the

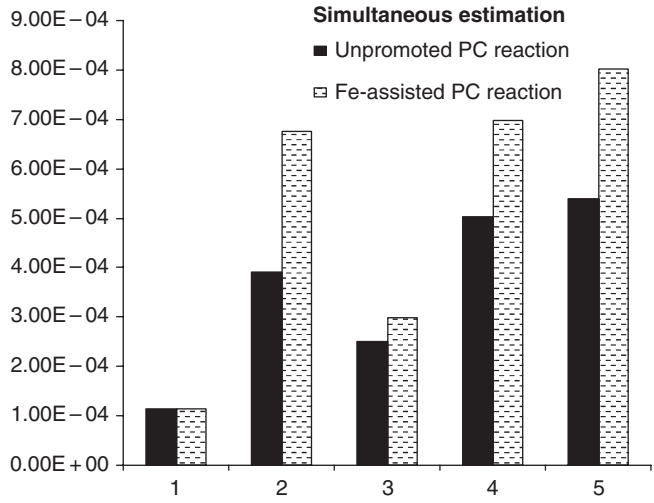

Figure 14 Estimates for simultaneous concentrations (20, 30, and 40 ppm C in phenol) (Ortiz-Gomez et al., 2008).

estimation of parameters in this new model. When the summation of the organic carbon due to the detected aromatic components (OC_{AR}) is compared with the TOC, it is observed that as the reaction proceeds both profiles divert from one another, as reported in Figure 15. The difference between these lines is employed to represent the amount of organic carbon contained in the carboxylic acids (OC_{AC}). Therefore, OC_{AC} can be calculated by subtracting OC_{AR} from TOC. If this amount is considered as a *lumped* concentration, a new kinetic model can be developed using this information.

Therefore, a number of relationships can be applied. The sum of all organic carbon (OC) in aromatics is given by

$$OC_{AR} = \sum_{i=1}^{n_A} C_{\text{aromatics}} \tag{19}$$

where n_A is the number of aromatics. Thus, the difference between TOC and OC_{AR} is the organic carbon due to carboxylic acids

$$OC_{Ac} = TOC - OC_{AR} \tag{20}$$

The amount of CO_2 produced during the course of the reaction is approximated by the difference between the initial concentration of total organic carbon and the concentration of TOC at any given time, as expressed in the following equation:

$$CO_2^{\text{Prod}} = [TOC_0] - [TOC] \tag{21}$$

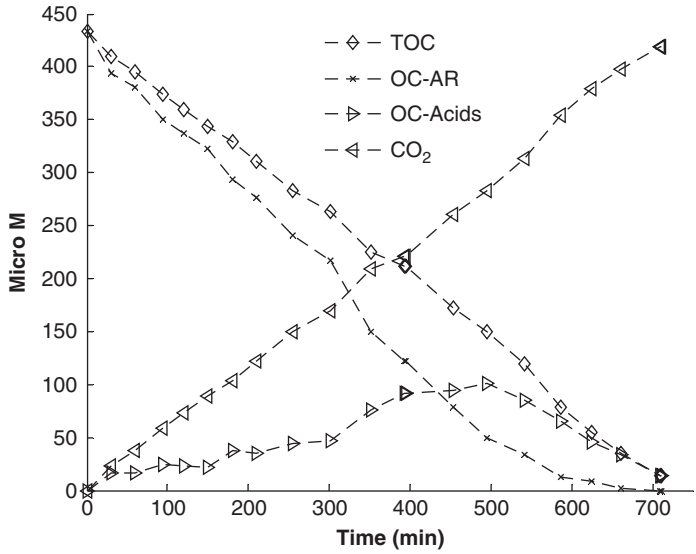

Figure 15 Comparison between OC_{AR} and TOC for the unpromoted PC oxidation of 30 ppm C in phenol. TOC and CO_2 profiles are in a different scale (six times higher than that shown on *Y*-axis) (Ortiz-Gomez et al., 2008).

where CO_2^{Prod} is the amount of CO_2 produced and $[TOC_0]$ is a vector containing the initial amount of TOC in all its elements. The number of data points for each experiment dictates its length. The CO_2^{Prod} profile is also shown in Figure 15. In Figure 15, both TOC and CO_2 profiles are reported in $\mu mol\,L^{-1}$ (μM) and are shown in a different scale for ease of comparison. The scale is six times higher than that shown on the *Y*-axis.

A summary of main assumptions for this model is as follows:

(a) 1,4-BQ and 1,2,4-THB terms are neglected.
(b) All carboxylic acids are *lumped* in one term
(c) All aromatic intermediates produce both carboxylic acids and CO_2 during the reaction.
(d) The amount of CO_2 produced is incorporated in the model. CO_2 is not adsorbed onto the catalyst surface and its concentration is considered to be cumulative throughout the course of the reaction.

Figure 16 shows a schematic representation of this new reaction network.

The estimation of parameters in this model was done testing different combinations to determine those parameters that were statistically significant and to obtain a kinetic model that could describe the experimental data over a wide range of concentrations with narrow CI. The model that provided the best estimates with the narrowest CI was obtained from the

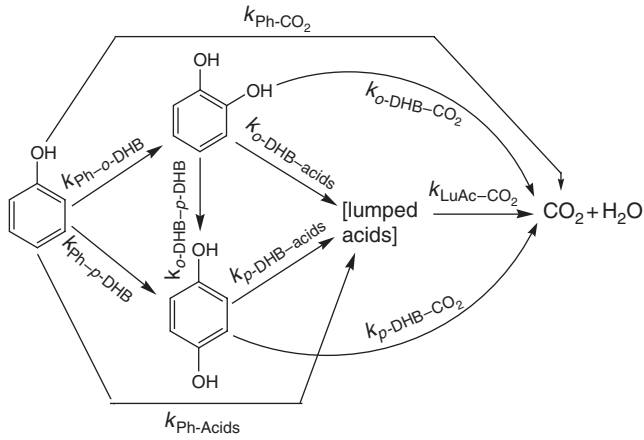

Figure 16 Schematic representation of reaction network for kinetic model #2 (KM#2) (Ortiz-Gomez et al., 2008).

reaction scheme presented in Figure 17. One can observe that some reaction steps have been neglected.

The results obtained with the simplified KM#2 for the unpromoted PC oxidation of phenol are shown in Figure 18a and b.

The concentration profiles for the same components are given when the estimation of parameters is performed for all 30, 40, and 50 ppm C in phenol. CO_2 profiles are shown in a different scale for ease of comparison. One can notice that the simplified KM#2 provides very good fitting for both single and simultaneous evaluations, which proves the validity of the model for the unpromoted PC oxidation of phenol.

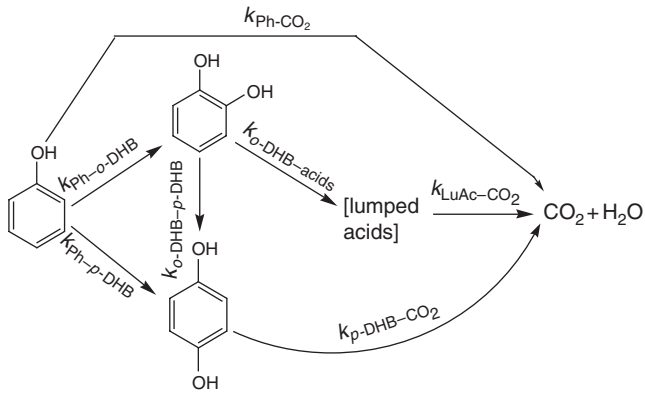

Figure 17 Reaction scheme obtained after testing various scenarios based on the original scheme used to develop kinetic model #2 (Ortiz-Gomez et al., 2008).

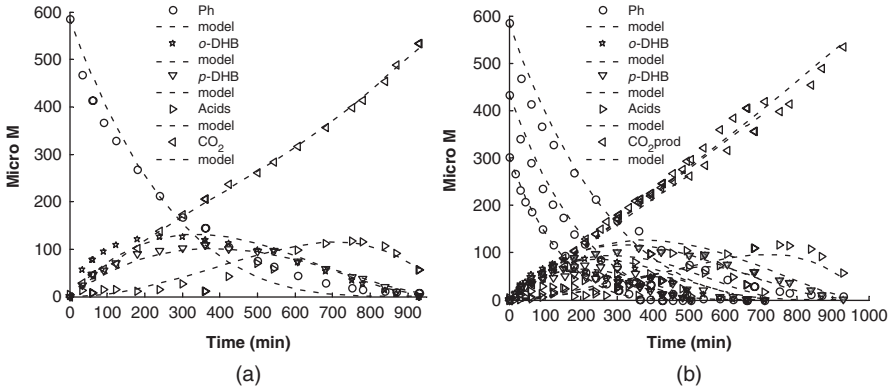

Figure 18 (a) Experimental and predicted profiles for the unpromoted PC oxidation of 40 ppm C in phenol using KM#2. (b) Experimental and predicted profiles for the unpromoted PC oxidation of 30, 40, and 50 ppm C in phenol using KM#2 (Ortiz-Gomez et al., 2008).

The statistically meaningful estimated parameters for this example are presented in Table 4. In this case, it was assumed that the adsorption constants for phenol, *o*-DHB, and *p*-HB were equal ($K^{A}_{Ph} = K^{A}_{p\text{-DHB}} = K^{A}_{o\text{-DHB}}$). All other combinations led to similar solutions with very wide CIs.

Likewise, the results using the simplified KM#2 for the estimation of parameters in the Fe-assisted PC reaction are reported in Figure 19. This figure shows the experimental and predicted concentration profiles obtained for the simultaneous evaluation of 30, 40, and 50 ppm C in phenol. It can be seen that the proposed model provides a good fit to the experimental data for this system as well. The estimated parameters and their corresponding CI for this case are given in Table 5.

Thus, it can be concluded that both KM#1 and KM#2 are adequate for a single concentration level or for wide range of concentrations, showing the usefulness of such models in the prediction of formation and disappearance of the model reactant and its oxidation intermediates. A comparison between the kinetic parameter estimates obtained for both unpromoted PC and Fe-assisted PC is given in Figure 20a and b. One can observe that the estimated parameters are close for most of the kinetic constants as predicted by the KM#2 model. This corroborates that this kinetic approach is suitable for the prediction of concentration profiles of phenol and its oxidation intermediates.

This section shows that both models such as KM#1 and KM#2 are suitable for the prediction of concentration profiles. Although many reaction intermediates are experimentally identified, not all of them can be included in the kinetic modeling due to their low concentrations and thus, their low

Table 4 Estimated parameters using reduced KM#2 for the simultaneous estimation of 30, 40, and 50 ppm C in phenol in the unpromoted PC oxidation

	Unpromoted PC oxidation	
	Simultaneous 30, 40, 50 ppm C in phenol	
	Estimate	CI
$k_{Ph \rightarrow CO_2}$ (1/min)	7.86e-04	6.66e-04
$k_{Ph \rightarrow o\text{-DHB}}$ (1/min)	9.58e-04	8.58e-04
$k_{Ph \rightarrow p\text{-DHB}}$ (1/min)	8.42e-04	7.92e-04
$k_{o\text{-DHB} \rightarrow LuAc}$ (1/min)	5.31e-04	4.13e-04
$k_{p\text{-DHB} \rightarrow CO_2}$ (1/min)	8.85e-04	7.52e-04
$k_{LuAc \rightarrow CO2}$ (1/min)	2.05e-04	1.75e-04
$K^A_{Ph}, K^A_{o\text{-DHB}}, K^A_{p\text{-DHB}}$ (1/μM)	7.23e-02	6.27e-02

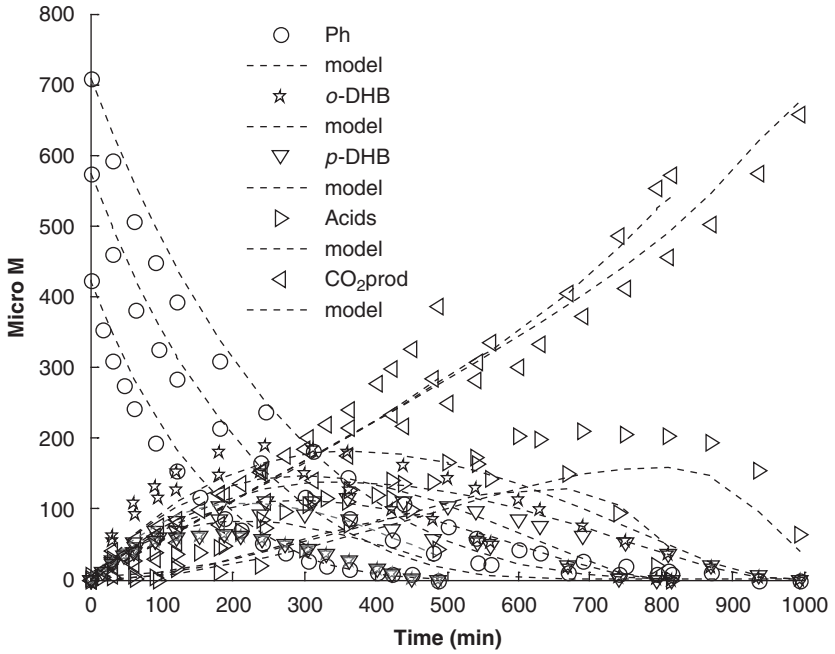

Figure 19 Experimental and predicted profiles for the Fe-assisted PC oxidation of 30, 40, and 50 ppm C in phenol using reduced KM#2 (Ortiz-Gomez et al., 2008).

significance in the parameter estimation. This shows as well that in cases like this, complex kinetic networks may be developed including all experimentally identified intermediates, but the kinetic models need to be

Table 5 Estimated parameters using reduced KM#2 for the Fe-assisted PC oxidation of 40 ppm C in phenol and for the simultaneous estimation of 30, 40, and 50 ppm C in phenol

	Fe-assisted PC oxidation	
	Simultaneous 30, 40, 50 ppm C in phenol	
	Estimate	CI
$k_{Ph \rightarrow CO_2}$ (1/min)	6.12e-04	5.03e-04
$k_{Ph \rightarrow o\text{-DHB}}$ (1/min)	1.30e-03	1.25e-04
$k_{Ph \rightarrow p\text{-DHB}}$ (1/min)	9.87e-04	7.92e-04
$k_{o\text{-DHB} \rightarrow LuAc}$ (1/min)	7.10e-04	4.56e-04
$k_{p\text{-DHB} \rightarrow CO_2}$ (1/min)	1.10e-03	8.58e-04
$k_{LuAc \rightarrow CO_2}$ (1/min)	2.60e-04	2.06e-04
$K^A_{Ph}, K^A_{o\text{-DHB}}, K^A_{p\text{-DHB}}$ (1/μM)	6.33e-03	5.47e-02

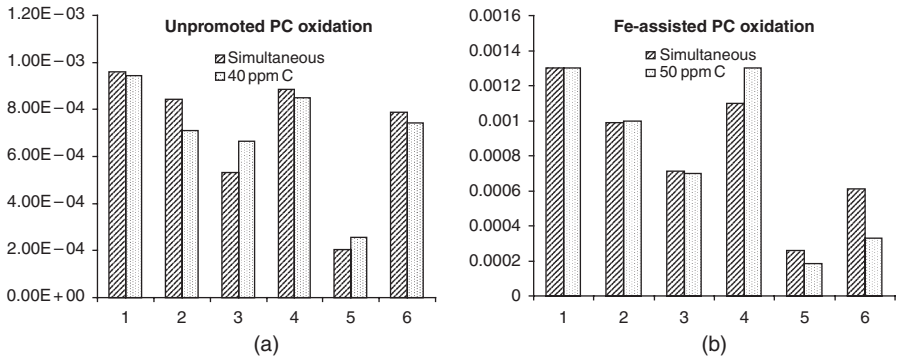

Figure 20 (a) Comparison between estimates obtained using KM#2 for unpromoted PC oxidation for 40 ppm C in phenol and simultaneous estimation. (b) Comparison between estimates obtained using KM#2 for Fe-assisted PC oxidation for 50 ppm C in phenol and simultaneous estimation (Ortiz-Gomez et al., 2008).

simplified due to the large number of parameters and their low statistical significance. It is clear that identifying as many reaction intermediates as possible helps understand the kinetic pathways but such information may not be readily applied in the development of kinetic models. Lastly, although these kinetic models are more comprehensive than those shown in other studies, they still need to be revisited to incorporate the effect of the radiation field in the kinetic constants so that they could be extensively used in reactor design.

5. CONCLUSIONS

The following are the main conclusions drawn from this study.

(a) It is shown that Fe cations have a strong influence on the phenol PC reaction. High concentrations lead to a decrease in the mineralization rates while low concentration promotes a significant increase. It is found that 5 ppm of Fe^{3+} ions renders the highest phenol oxidation rate. Moreover, it is demonstrated that ferric ions Fe^{3+} and ferrous ions Fe^{2+} promote the same enhancement. It is proposed that Fe cations increase the mineralization rate by facilitating the transfer of photogenerated electrons e_{cb}^{-} to electron scavengers. This occurs through a continuous oxidation–reduction cycle of Fe cations adsorbed onto the catalyst surface.

(b) Additionally, it is demonstrated that the Fe-assisted PC oxidation of phenol can be represented with a series–parallel kinetic reaction scheme. Likewise, the Fe-assisted PC oxidations of reaction intermediates *o*-DHB, *p*-DHB, and 1,4-BQ can be represented with a series–parallel reaction network. An overall kinetic reaction scheme for the Fe-assisted PC reaction of phenol is proposed. Its similarities and differences with that derived for the unpromoted PC reaction, as well as the main contributions, are discussed in detail.

(c) Lastly, a kinetic model based on the overall kinetic reaction network proposed for both unpromoted PC reaction and Fe-assisted PC reaction is developed using LH-type kinetics for each chemical species. Given that the concentrations of some of the intermediates in both systems are very small, this allows the simplification of the overall kinetic model. Subject to simplifying assumptions, two simplified models (KM#1 and KM#2) are obtained.

(d) The KM#1 is developed to predict the rate of reaction of phenol and its major aromatic intermediates. A parameter representing the ratio of *o*-DHB converted into *p*-DHB to *o*-DHB converted into acids and CO_2 was incorporated in the kinetic model originally presented by Salaices et al. (2004). This parameter was represented as *R*. The resulting model provided very good and statistically meaningful fitting for both unpromoted PC and Fe-assisted PC oxidations. In this case, the estimated parameters are consistent with the experimental data, with the parameters from the Fe-assisted PC reaction being larger than those of the unpromoted PC system.

(e) The KM#2 is developed considering a lumped acid concentration and the formation of CO_2. This model predicts the formation and disappearance of aromatic intermediates, carboxylic acids, and CO_2 in the course of the PC reaction. It provides very good fit of the experimental data and works very well for a wide range of phenol concentrations (20–50 ppm C in phenol). The estimated parameters in this case are also consistent with the experimental data.

(f) In this study, it was demonstrated that an environmentally friendly and highly abundant metal such as Fe could be readily used for the enhancement of the mineralization rates of a wide variety of recalcitrant organic pollutants.

RECOMMENDATIONS

Based on the assertions above, various recommendations could be outlined for future work in this research area. The method employed for the enhancement of PC oxidation and the type of the reactors used, albeit low cost, present two significant limitations: loss of catalyst and use of UV radiation for catalyst activation. Therefore, two major areas must continue to receive special attention: catalyst recovery and use of visible radiation to make use of an inexhaustible radiation source, the solar radiation.

To increase catalyst recovery, efforts have been directed toward immobilization of the photocatalyst on a wide variety of materials. However, there is an inherent decrease of catalytic activity due to a reduced surface area. As such, Fe could be used to minimize or compensate for the catalyst deactivation due to the support preparation. New methods must be developed to ensure Fe ions stay adsorbed onto the photocatalyst surface to avoid further reactivation posttreatments.

Regarding the use of solar radiation, new materials including doped TiO_2, capable of being activated with visible irradiation, must be developed. Development of photocatalysts with such features will undoubtedly help take advantage of the large regions with high solar radiation intensities. Also careful attention should be given to the feasibility of using sophisticated catalyst-doping procedures in the preparation of these improved semiconductor materials.

LIST OF SYMBOLS

Variables

C	Pollutant concentration, μM
r_i	Rate of reaction, μ mol/(g_{cat} min)
R	Ratio of k_o-$_{DHB \rightarrow CO_2}$ to k_o-$_{DHB \rightarrow p\text{-}DHB}$
t	Time, min
V	Volume, L
V_{CST}	Volume of CST, L
V_{PFR}	Volume of PFR, L
W	Weight of catalyst, g

Parameters

k	Apparent kinetic constant
k^{I}	Intrinsic kinetic constant
k^{k}	Kinetic constant, $M/(g_{cat}\ min)$
K^{A}	Adsorption constant $l/\mu M$

Subscripts

Ac	Carboxylic acids
CO_2	Carbon dioxide
FoAc	Formic acid
FuAc	Fumaric acid
1,2,4-THB	1,2,4-Trihydroxybenzene
1,4-BQ	1,4-Benzoquinone
i	Chemical species
j	Chemical species
MeAc	Maleic acid
Ph	Phenol
OxAc	Oxalic acid
o-DHB	*ortho*-dihydroxybenzene
p-DHB	*para*-dihydroxybenzene
CST	Continuous stirred tank
PFR	Plug flow reactor

Acronyms

1,4-BQ	1,4-Benzoquinone
1,2,3-THB	1,2,3-Trihydroxybenzene
1,2,4-THB	1,2,4-Trihydroxybenzene
CI	Confidence intervals
Fe-assisted PC	Photocatalytic reaction assisted with Fe ions
HPLC	High-performance liquid chromatography
KM#1	Kinetic model #1
KM#2	Kinetic model #2
Unpromoted PC	Photocatalytic reaction in the absence of Fe ions.
OQY	Overall quantum yield
o-DHB	*ortho*-dihydroxybenzene
p-DHB	*para*-dihydroxybenzene
ppm C	Parts per million of carbon
Photo-CREC	Chemical reactor designed at the Chemical Reaction Engineering Centre
PC	Photocatalytic
TOC	Total organic carbon
TiO_2	Titanium dioxide
UV	Ultraviolet

REFERENCES

Agency for Toxic Substances and Disease Registry (ATSDR). Public Health Service, US Department of Health and Human Services, Atlanta, GA (1998).

Aguado, M.A., Cervera-March, S., and Gimenez, J. *Chem. Eng. Sci.* **50**(10), 1561 (1995).

Aguado, J., Grieken, R.V., López-Muñoz, M.J., and Marugán, J. *Catal. Today* **75**, 95 (2000).

Al-Ekabi, H., and Serpone, N. *J. Phys. Chem.* **92**, 5726 (1988)

Al-Ekabi, H., Serpone, N., Pelizzetti, E., Minero, C., Fox, M.A., and Draper, B.R. *Langmuir* **5**, 250 (1989).

Araña, J., González, O., Doña, J.M., Herrera, J.A., Garriaga, C., Pérez, J., Carmen, M., and Navío-Santos, J. *J. Mol. Catal. A: Chem.* **197**, 157 (2003).

Araña, J., González, O., Doña, J.M., Herrera, J.A., Tello Rendon, E., Navío-Santos, J., and Perez Peña, J. *J. Mol. Catal. A: Chem.* **215**, 153 (2004).

Araña, J., González, O., Miranda, M., Doña, J.M., and Herrera, J.A. *Appl. Catal. B: Environ.* **36**, 113 (2002).

Araña, J., González, O., Miranda, M., Doña, J.M., Herrera, J.A., and Pérez, J. *Appl. Catal B: Environ.* **36**, 49 (2001).

Assabane, A., Ichou, Y.A., Tahiri, H., Guillard, C., and Herrmann, J.M. *Appl. Catal. B: Environ.* **24**, 71 (2000).

Bahnemann, D. *Solar Energy* **77**, 445 (2004).

Bamwenda, G.R., Tsubota, S., Nakamura, T., and Haruta, M. *J. Photochem. Photobiol. A: Chem.* **89** (1995).

Blake, Daniel. M., Bibliography of work on the Heterogeneous Photocatalytic removal of Hazardous Compounds from Water and Air, National Renewable Energy Laboratory (NREL). Update No. 4 to October (2001).

Bouquet-Somrani, C., Finiels, A., Graffin, P., and Olivé, J.L. *Appl. Catal. B: Environ. B* **8**, 101 (1996).

Carraway, E.R., Hoffman, A.J., and Hoffman, M.R., *Environ. Sci. Tech.* **28**, 766 (1994).

Cermenati, L., Pichat, P., Guillard, C., and Albini, A. *J. Phys. Chem. B* **101**, 2650 (1997).

Chen, D., and Ray, A.K. *Water Res.* **32**, 11, 3223 (1998).

Chen, D., and Ray, A.K. *Appl. Catal. B* **23**, 143 (1999).

Chen, D., and Ray, A.K. *Chem. Eng. Sci.* **56**, 1561 (2001).

Chenthamarakshan, C.R., and Rajeshwar, K. *Langmuir* **16**, 2715 (2000).

Chenthamarakshan, C.R., and Rajeshwar, K. *Electrochem. Comm.* **2**, 527 (2002).

Colmenares, J.C., Aramendia, M.A., Marinas, A., Marinas, J.M., and Urbano, F.J. *Appl. Catal. A: Gen.* **306**, 120 (2006).

Colon, G., Hidalgo, M.C., and Navío, J.A. *J. Photochem. Photobiol. A: Chem.* **138**, 78 (2001).

Cotton, F.A., Wilkinson, G., Murillo, C., and Bochmann, M. "Advanced Inorganic Chemistry", Chapter 17, Wiley, New York (1999), p. 692.

Dai, Q., and Rabani, J. *J. Photochem. Photobiol. A: Chem.* **148**, 17 (2002).

de Lasa, H., Serrano, B., and Salaices, M. "Photocatalytic Reaction Engineering". Springer, New York (2005).

Domenech, X., Jardim, W.F., and Litter, M.I. Advanced oxidation Processes for Contaminant Elimination. *in* M.A. Blesa, and B. Sánchez (Eds.), "Elimination of Contaminants Through Heterogeneous Photocatalysis", CIEMAT (2004).

Englezos, P., and Kalogerakis., N. "Applied Parameter Estimation for Chemical Engineers", Chapter 2, 7 Marcel Dekker, Inc. New York (2001).

Fox, M.A. *in* N. Serpone, and E. Pelizzeti (Eds.), "Photocatalysis – Fundamentals and Applications". Wiley-Interscience, New York (1990), p. 421.

Franch, M.I. Ayllón, A.J., Peral, J., and Domenech, X. *Catal. Today* **101**, 245 (2005).

Fujishima, A., Rao, T.N., and Tryk, D.A. *J. Photochem. Photobiol. C: Photochem. Rev.* **1**, 1 (2000).

Goi, A., and Trapido, M. *Proc. Estonian Acad. Sci. Chem.* **50**(1), 5 (2001).

Grela, M.A., Coronel, M.E.J., and Colussi, A.J., *J. Phys. Chem.* **100**, 16940 (1996).
Guillard, C. *J. Photochem. Photobiol. A.* **158**, 27 (2003).
Herrmann, J.M. *Catal. Today* **53**, 115 (1999).
Huang, M., Tso, E., Datye, A.K., Prairie, M.R., and Stange, B.M. *Environ. Sci. Tech.* **30**, 3084 (1996).
Hufschmidt, D., Bahnemann, D., Testa, J.J., Emilio, C.A., and Litter, M.I. *J. Photochem. Photobiol. A: Chem.* **148**, 223 (2002).
Jakob, L., Hashem, T.M., Burki, S., Guindy, N., and Braun, A.M. (1993a).
Jakob, L., Oliveros, E., Legrini, O., and Braun, A.M. *in* Ollis, D., and Al-Ekabi, H. (Eds.), "Photocatalytic Purification and Treatment of Water and Air". Elsevier, New York (1993b), p. 511.
Karamanev, D.G., Nikolov, L.N., and Mamatarkova, V. *Min. Eng.* **15**, 341 (2002).
Karvinen, S., and Lamminmaki, R.-J. *Solid State Sci.* **5**, 1159 (2003).
Kavitha, V., and Palanivelu, K. *Chemosphere* **55**, 1235 (2004).
Kim, T.K., Lee, M.N., Lee, S.H., Park, Y.C., Jung, C.K., and Boo, J.H. *Thin Solid Films* **475**, 171 (2005).
Leyva, E., Moctezuma, E., Ruíz, M.G., and Torres-Martinez, L. *Catal. Today* **40**, 367 (1998) .
Li, X., Cubbage, J.W., Jenks, and W.S. *J. Org. Chem.* **64**, 8525 (1999b).
Li, X., Cubbage, J.W., Tetzlaff, T.A., and Jenks, W.S. *J. Org. Chem.* **64**, 8509 (1999a).
Li Puma, G, and Lock Yue, P., *Ind. Eng. Chem. Res.* **38**, 3246 (1999).
Malato, S., Blanco-Galvez, J., and Estrada-Gasca, C. *Photocatal. Guest Editorial Solar Energy* **77**, 443 (2004).
Mathews, R.W., and McEvoy, S.R. *Solar Energy* **49**(6), 507 (1992).
McDonald, T.A., Holland, N.T., Skibola, C., Duramad, P., and Smith, M.T. *Leukemia* **15**, 10 (2001).
Minero, C., Catozzo, F., Pelizzetti, E. *Langmuir*, **8**, 481 (1992).
Mukherjee, P.S., and Ray, A.K. *Chem. Eng. Tech.* **22**(3), 253 (1999).
Nagaveni, K., Hegde, M.S., and Madras, G. *J. Phys. Chem. B* **108**, 20204 (2004).
Navío, J.A., Colón, G., Litter, M.I. and Bianco, G.N. *J. Mol. Catal. A: Chem.* **106**, 267 (1996).
Navío, J.A., Testa, J.J., Djedjeian, P., Padrón, J.R., Rodríguez, D., and Litter, M. *Appl. Catal. A: Gen.* **178**, 191 (1999).
Oh, S.M., Kim, S.S., Lee, J.E., Ishigaki, T., and Park, D.W. *Thin Solid Films* **435**, 252 (2003).
Okamoto, K., Yamamoto, Y., Tanaka, H., and Tanaka, M. *Bull. Chem. Soc. Jpn.* **58**, 2015 (1985).
Ollis, D.F., Pelizzeti, E., and Serpone, N. *in* N. Serpone, and E. Pelizzeti (Eds.) "Photocatalysis Fundamentals and Applications". Wiley Interscience, New York (1989), p. 603.
Ortiz-Gomez, A. Ph.D., "Enhanced Mineralization of Phenol and other Hydroxylated Compounds in a Photocatalytic Process assisted with Ferric Ions". Thesis Dissertation, The University of Western Ontario, Ontario (2006).
Ortiz-Gomez, A., Serrarro-Rosales, B., and de Lasa, H. *Chem. Eng. Sci.* **63**, 520 (2008).
Ortiz-Gomez, A., Serrano-Rosales, B., Salaices, M., and de Lasa, H. *Ind. Eng. Chem. Res.* **46**, 23, 7394 (2007).
Pellizetti, E. *Solar Energy Mater. Solar Cells* **38**, 453 (1995).
Pichat, P. *Water Sci. Tech.* **4**, 73 (1997).
Pignatello, J.J., Liu, D., and Huston, P. *Environ. Sci. Tech.* **33**, 1832 (1999).
Poulopoulos, S.G., and Philippopoulous, C.J. *J. Environ. Sci. Health A* **39**(6), 1385 (2004).
Preis, S., Terentyeva, Y., and Rozkov, A. *Water. Sci. Tech.* **35**(4), 165 (1997).
Ray, A.K. *Dev. Chem. Eng. Mineral. Proc.* **5**(1/2), 115 (1997).
Riegel, G., and Bolton, J.R. *J. Phys. Chem.* **99**(12), 4215 (1995).
Rothenberger, G., Monser, J., Gratzel, M., Serpone, N., and Sharma, D.K. *J. Am. Chem. Soc.* **107**, 8054 (1985).
Salaices, M., Serrano, B., and de Lasa, H. *Chem. Eng. Sci.* 59, 3 (2004).
Sokmen, M., and Ozkan, A. *J. Photochem. Photobiol. A.* **147**, 77 (2002).

Stylidi, M., Kondaridis, D.I., and Verykios, X.E. *Appl. Catal. B: Environ.* **40**, 271 (2003).
Tan, T., Beydoun, D., and Amal, R. *J. Photochem. Photobiol. A.* **159**, 273 (2003).
Trillas, M., Pujol, M., and Doménech, X. *J. Chem. Tech. Biotech.* **55**, 85 (1992).
Tryba, B., Morawski, A.W., Inagaki, M., and Toyoda, M. *Appl. Catal. B: Environ.* **63**, 215 (2006a).
Tryba, B., Morawski, A.W., Inagaki, M., and Toyoda, M. *J. Photochem. Photobiol. A: Chem.* **179**, 224 (2006b).
Tseng, J., and Huang, C.P. Mechanistic aspects of the photocatalytic oxidation of phenol in aqueous solutions. *in* D.W. Tedder, and F.G. Pohland (Eds.), "Emerging Technologies in Hazardous Waste Management", Chapter 2. Amer. Chem. Soci., Washington, DC, (1990), pp. 12–39.
Turchi, C.S., and Ollis, D.F. *J. Catal.* **119**, 483 (1989).
Turchi, C.S., and Ollis, D.F. *J. Catal.* **122**, 178 (1990).
US Environmental Protection Agency. "Phenol-Hazard Summary". Reviewed on 2000. US Environmental Protection Agency website (www.epa.gov) (2000).
Vamathevan, V., Amal, R., Beydoun, D., Low, G., and McEvoy, S. *J. Photochem. Photobiol. A: Chem.* **148**, 233 (2002).
Wei, T.Y., and Wan, C., *J. Photochem. Photobiol. A: Chem.* **69**, 241 (1992).
Winterbottom, J.M., Khan, Z., Boyes, A.P., and Raymahasay, S. *Environ. Prog.* **62**, 125 (1997).
Wolfrum, E.J., and Turchi, G.S. *J. Catal.* **136**, 626 (1992).
Wyness, P., Klausner, J.F., and Goswami, D.Y. *J. Solar Energy Eng.* **116**, 8 (1994).
Yang, S., Lou, L., Wang, K., and Chen, Y. *App. Catal. A: Gen.* **301**, 152 (2006).
Zepp, R.G., Faust, B.C., and Holgne, J. *Environ. Sci. Tech.* **26**, 313, (1992).
Zertal, A., Molnár-Gábor, D., Malouki, M.A., Shili, T., and Boule, P. *Appl. Catal. B: Environ.* **49**, 83 (2004).
Zhou, J., Zhang, Y., Zhao, X.S., and Ray, A.J. *Ind. Eng. Chem. Res.* **45**, 3503, (2006).